Energy Reports 15 (2026) 108997



Contents lists available at ScienceDirect

Energy Reports

journal homepage: www.elsevier.com/locate/egyr



Research paper



Towards reliable solar power forecasting in Sub-Saharan Africa: An explainable hybrid AI approach for Chad

Alpaslan Demirci [a], Idriss Dagal [b], Musa Terkes [a], Umit Cali [c,d,*]

[a] Department of Electrical Engineering, Yildiz Technical University, 34220 Istanbul, Türkiye
[b] Department of Electrical-Electronics Engineering, Istanbul Beykent University, 34396 Istanbul, Türkiye
[c] Department of Electric Power Engineering, Norwegian University of Science and Technology, 7034 Trondheim, Norway
[d] School of Physics, Engineering and Technology, University of York, YO10 5DD York, United Kingdom

ARTICLE INFO

Keywords:
Solar forecasting
LSTM
XGBoost
Explainable AI
Sub-Saharan Africa
Chad

ABSTRACT

Reliable solar power forecasting is critical for expanding energy access and maintaining grid stability in Sub-Saharan Africa, where electrification rates remain low and climatic variability is substantial. This paper introduces one of the first systematic AI-based forecasting studies for Chad, employing a hybrid architecture that integrates Long Short-Term Memory (LSTM) with attention and Extreme Gradient Boosting (XGBoost). Leveraging hourly PV and meteorological data from three representative cities (Pala, Mao, and Amdjarass) across the Sudanian, Sahelian, and Saharan zones, the framework demonstrates forecasting errors consistently below 3% of average hourly PV output. Model interpretability, provided through SHAP analysis, underscores solar irradiance, temperature, and temporal indicators as dominant features, thereby strengthening transparency and user confidence. The findings extend beyond methodological contributions by revealing region-specific dynamics: rainfall-induced fluctuations in Sudanian areas highlight the need for storage and backup capacity, while the stable Saharan climate favors large-scale PV integration. By translating forecasting accuracy into practical design and policy implications, the study supports mini-grid planning, investment prioritization, and fossil-fuel displacement. These outcomes align with global sustainability objectives and highlight the role of explainable AI in enabling resilient and equitable electrification pathways in data-scarce regions.

1. Introduction

Chad, a landlocked country in Africa's Sahel region, faces significant challenges due to diverse climatic conditions and the impact of climate variability on socio-economic development (Muh and Tabet, 2019; Anon, 2024). The country's climate ranges from arid deserts in the north to more humid savannas in the south, reflecting substantial regional differences (Allarané et al., 2024). Understanding and predicting these climatic variations is critical for sustainable development (Ahmed et al., 2024), particularly in sectors such as agriculture and energy that are highly dependent on climatic conditions (Mirzania et al., 2023; Mellit and Kalogirou, 2023). This study aims to comprehensively assess and predict climate variability across different regions of Chad, with a particular focus on solar radiation and temperature dynamics, emphasizing their implications for energy production potential and sustainable development. These two parameters not only directly affect the country's agricultural productivity but also determine the potential for harnessing solar energy, a key component in strategies to enhance energy security and diversify resources (Souloukngа et al., 2017; Goni et al., 2019). The fight against desertification has spurred a crucial transition toward renewable energy. In this context, accurate wind resource modeling using statistical approaches such as the Weibull distribution has proven effective for evaluating wind potential in rural areas (Hossen et al., 2022; Bernard et al., 2024).

The heavy reliance on primary energy sources such as wood and charcoal has become unsustainable due to widespread deforestation. Recent studies emphasize the need for statistical characterization of solar resources in arid and semi-arid regions such as Chad (Liu et al., 2024; Mutavhatsindi et al., 2020). Similar restrictions on biomass access in East African nations accelerated the shift toward renewable energy (Sisay et al., 2023). However, the transition to butane gas posed challenges due to high costs and limited accessibility. Recent works highlight solar energy as a cost-effective and reliable alternative, especially for thermal needs at the household level in off-grid areas (Otieno et al., 2023; Bouhorma et al., 2023). As a clean and inexhaustible source, solar energy holds immense potential for meeting

* Corresponding author at: Department of Electric Power Engineering, Norwegian University of Science and Technology, 7034 Trondheim, Norway.
E-mail address: umit.cali@ntnu.no (U. Cali).

https://doi.org/10.1016/j.egyr.2025.108997
Received 26 September 2025; Received in revised form 5 December 2025; Accepted 23 December 2025
2352-4847/© 2026 The Authors. Published by Elsevier Ltd. This is an open access article under the CC BY-NC-ND license (http://creativecommons.org/licenses/by-nc-nd/4.0/).

household and business energy needs in Chad, with both economic and environmental benefits (Kriga et al., 2023; Smith et al., 2023). For example, solar stove field trials in Sub-Saharan Africa have demonstrated significant reductions in household fuel costs (McCann et al., 2024). Sub-Saharan Africa, despite its abundant renewable energy potential, continues to face a critical energy crisis due to low electricity access (Mukhtar et al., 2023). Rural energy access remains constrained, yet new solar mini-grid projects in Kenya and Nigeria have improved living standards and reduced dependence on solid fuels (Carabajal et al., 2024). While renewable energy has the potential to enhance economic growth and improve quality of life, its adoption is hindered by multiple barriers (Kumar and Umanand, 2005).

Chad continues to struggle with severe electricity shortages for households and businesses (Hassan et al., 2016). To address this, the government and the energy sector are collaborating to promote solar energy as a viable alternative that provides locally adapted solutions. These initiatives aim to reduce reliance on fossil fuels, particularly in rural areas, while fostering self-employment and supporting livelihoods through clean energy planning (Kabeer et al., 2023). Understanding energy demand and resource availability is critical for optimizing solar and wind systems. Chad benefits from abundant solar and wind resources, particularly in its northern and central regions, yet this potential remains largely untapped. Solar irradiance modeling in arid West Africa must account for desert dust aerosols, which significantly reduce direct solar radiation levels (Xiao et al., 2025). Similarly, wind resource assessments using ERA5 reanalysis data provide a robust foundation for site-specific energy planning in Chad's wind-rich zones (Doe and Smith, 2024). Harnessing this clean energy potential requires careful analysis of optimal system sizing, considering sunshine duration, wind speeds, and local electricity demand across regions (Ghaderian et al., 2020). A comprehensive assessment of the spatial and temporal variations of solar radiation and temperature across Chad's diverse geographical regions is conducted using historical data, satellite observations, and climate modeling techniques. The study identifies distinct climate regions, examines seasonal and interannual variations, and highlights zones with the highest solar potential and those most vulnerable to temperature fluctuations (Zhang et al., 2024; Singh et al., 2023; Mostafaeipour et al., 2020).

The predictive dimension of this study is particularly important, as it projects future climate scenarios by considering both natural variability and the potential impacts of global climate change, especially on photovoltaic energy potential in Sub-Saharan Africa (Teal et al., 2024b). Coupled Model Intercomparison Project Phase 6 projections highlight potential shifts in solar energy availability, particularly in regions sensitive to atmospheric and radiative changes (Teal et al., 2024a). Accurate modeling of direct and diffuse solar radiation is critical for solar energy simulations and long-term planning, as validated by multi-year studies (Ineichen, 2023; Pereira et al., 2024). These projections are crucial not only for designing adaptive strategies to mitigate adverse impacts on agriculture, water access, and public health, but also for developing long-term strategies for the optimal utilization of solar technologies (Koshkarbay et al., 2024).

Therefore, this research aims to bridge the gap between climate science and practical energy forecasting applications, providing policymakers, energy planners, and regional stakeholders with reliable and interpretable insights. By leveraging 20 years of meteorological and photovoltaic (PV) data across Chad's diverse climatic zones, the proposed hybrid LSTM–Attention and XGBoost framework enables both detailed characterization of climate variability and highly accurate photovoltaic power forecasts. Enhanced with SHAP-based interpretability to improve transparency, this approach contributes to the development of adaptive climate strategies, the reinforcement of grid reliability, and the advancement of sustainable energy planning in Sub-Saharan Africa.

1.1. Literature review

The global energy transition has accelerated the shift from fossil-based generation to renewable sources, with solar energy playing a central role due to its abundance, sustainability, and economic feasibility (Li et al., 2020b,a). PV systems are increasingly integrated into modern power grids, supporting climate change mitigation and sustainable development objectives (Akhter et al., 2022; Keddouda et al., 2023). However, the inherent intermittency of PV generation, driven by atmospheric conditions, introduces uncertainty in balancing supply and demand, grid stability, and operational planning (Zhang et al., 2023). Consequently, accurate PV forecasting has become indispensable for grid management, reserve allocation, and energy market operations (AlKandari and Ahmad, 2020; Hossain et al., 2021). In this direction, the traditional statistical models, such as Seasonal AutoRegressive Integrated Moving Average (SARIMA), have been employed for PV forecasting but often fall short in capturing the nonlinear and stochastic nature of solar irradiance. Machine learning and deep learning (DL) methods have gained prominence, offering improved accuracy and robustness (Wentz et al., 2022; Zheng et al., 2023). Convolutional neural networks (CNN), long short-term memory (LSTM), gated recurrent units (GRU), and Transformer architectures demonstrate strong capability in modeling spatiotemporal dependencies (Agga et al., 2022; Riedel et al., 2024). Attention mechanisms and temporal encodings further enhance these models by effectively learning long-term dependencies (Geng et al., 2023; Nam et al., 2025). To increase prediction accuracy, hybrid approaches have combined frequency-domain decomposition methods (ensemble empirical mode decomposition), complete ensemble empirical mode decomposition with adaptive noise (CEEMDAN), variational mode decomposition, dimensionality reduction, feature selection (Least Absolute Shrinkage and Selection Operator (LASSO), SHapley Additive exPlanations (SHAP)), and hyperparameter optimization algorithms (Bayesian optimization, grey wolf optimization (GWO), improved salp swarm algorithm (ISSA)) (Zhang et al., 2023; Wang et al., 2023; Talaat et al., 2022). Ensemble frameworks (extreme gradient boosting (XGBoost), light gradient boosting machine, categorical boosting) have also been integrated with DL architectures, leveraging the complementary strengths of multiple models (Li et al., 2022; Kim et al., 2023; Ghimire et al., 2022). More recently, uncertainty quantification, synthetic data generation using generative adversarial networks (GAN), and explainable AI techniques have been introduced to address data scarcity, improve model generalization, and enhance interpretability of model decisions (Wentz et al., 2022; Mubarak et al., 2023).

Despite these global advancements, research on renewable energy in Chad remains relatively limited and fragmented. Early studies primarily assessed solar energy potential for specific regions such as Mongo and Pala using NASA and PVGIS data from 2010–2020 (Nsafon et al., 2020). Graphical and statistical analyses revealed sinusoidal patterns in monthly irradiance and nonlinear hysteresis-like relationships with temperature. The maximum entropy principle was employed to identify irradiance peaks in March, while the lowest values were observed in August. These insights proved useful for PV system design, though reliance on monthly data limited the precision of frequency distributions. Subsequent comparative studies further confirmed that Pala generally exhibits higher irradiance than Mongo, especially in March and April, underscoring its suitability for PV deployment (Soulouknga et al., 2022). Broader analyses addressed limitations of prior work by expanding the scope to 16 unelectrified regions of Chad. Other works employed geographic information system-based techniques such as the inverse distance weighted interpolation and Weibull distribution to map both solar and wind resources. Results highlighted higher solar potential in Pala and stronger wind speeds in Faya-Largeau, with wind energy potential more geographically constrained (Jahangiri et al., 2019). Using NASA's POWER database, a comprehensive dataset (2010–2021) was compiled to categorize Chad into three distinct climatic zones:

- **Sahelian Region:** Regions such as Mao, Bol, and Mongo peak between March and May, with December as the minimum month.
- **Saharan Zone:** Locations including Amdjarass, Bardai, and Fada record the lowest irradiation in January, with sharp increases between April and June.
- **Sudanian Zone:** Areas such as Pala, Lai, Am-Timan, and Koumra peak in April, with minima in December.

These studies provided essential baseline insights into Chad's renewable energy landscape. However, their reliance on monthly averaged data restricted the ability to capture intraday variability, which is crucial for PV power forecasting and operational planning. Despite these baseline contributions, a significant research gap persists in the Sub-Saharan African context, particularly for Chad. Most prior studies have focused on resource mapping and techno-economic feasibility assessments using coarse temporal resolutions (monthly or daily averages), which are insufficient to capture short-term PV generation dynamics. Moreover, reliable solar power forecasting research in Africa remains scarce compared to Asia, Europe, and North America, largely due to limited ground measurements, fragmented datasets, and infrastructural challenges. This scarcity hampers the development of robust, data-driven forecasting frameworks that can support grid integration, demand–supply balancing, and energy access planning in regions with already fragile electricity infrastructures. Addressing this gap requires shifting the focus from static potential assessments toward dynamic, explainable forecasting approaches that are tailored to Africa's unique climatic and socio-economic contexts.

The reviewed literature highlights two important observations. First, global PV forecasting research has shifted toward hybrid AI-based models with uncertainty quantification and explainability. Second, studies in Chad remain largely resource-mapping oriented, focusing on spatial and seasonal solar potential rather than short-term predictive modeling. Addressing this gap, the present study integrates long-term historical datasets with a hybrid LSTM–XGBoost framework to perform short-term PV power forecasting enriched with explainability. This transition from static resource characterization to dynamic predictive modeling offers a more practical contribution to system planning, grid integration, and reliable energy management in Chad's diverse climatic zones. Fig. 1 presents the map of Chad, illustrating the three major climatic zones along with the representative cities located within each region.

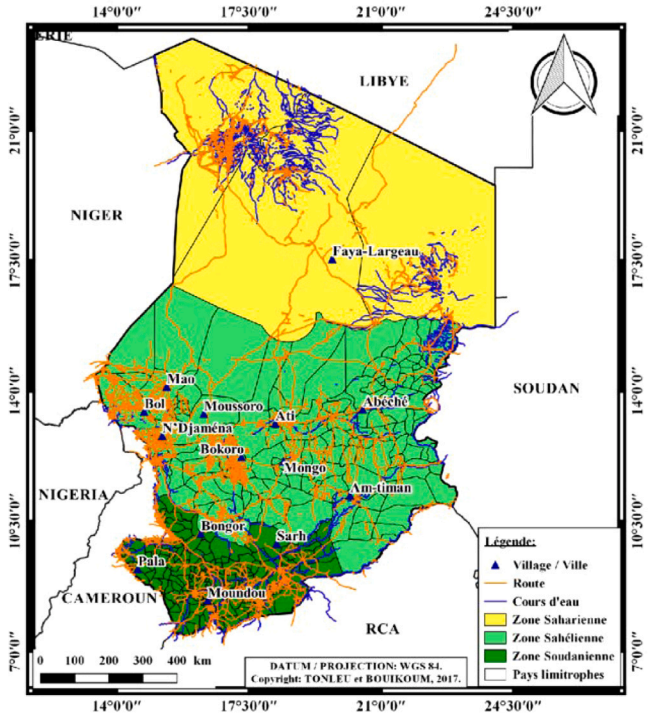


Fig. 1. Climatic zoning of Chad into Sudanian, Sahelian, and Saharan regions.

1.2. Positioning within contemporary hybrid PV forecasting literature

Recent advances in solar forecasting have increasingly explored hybrid modeling paradigms that integrate DL with tree-based or ensemble approaches. Existing work commonly couples LSTM networks with gradient-boosting models, random forests, or statistical post-processors to leverage complementary strengths in temporal representation and nonlinear feature partitioning. Despite these developments, hybrid frameworks remain predominantly evaluated in high-data, infrastructure-rich regions such as Europe, North America, and East Asia, where high-quality irradiance measurements and dense sensor networks substantially simplify the forecasting task.

The approach developed in this study differs from contemporary hybrid formulations in several important respects. First, the architecture integrates an attention-augmented LSTM with an XGBoost residual learner, enabling the model to jointly capture multiscale temporal dependencies and localized nonlinear interactions that arise in the highly variable Sahelian irradiance regime. Unlike conventional serial or ensemble hybrids, the proposed system uses XGBoost to explicitly model structured residual patterns left unaddressed by the deep sequence encoder, thereby enhancing performance during abrupt irradiance transitions commonly driven by dust, aerosols, and convective clouds. Second, while many recent hybrid models rely on dense auxiliary data (e.g., sky images, numerical weather predictions, satellite-based cloud motion fields), the framework presented here is deliberately designed for low-infrastructure contexts. It operates exclusively on ground-based meteorological and irradiance measurements and applies uncertainty quantification methods tailored for data-scarce regions. This contrasts with most state-of-the-art hybrid approaches, whose reliance on extensive upstream inputs limits their applicability in remote African settings.

Finally, the study represents one of the few works to systematically evaluate hybrid PV forecasting models across multiple climatic zones within Sub-Saharan Africa, providing evidence on geographic transferability, domain adaptation behavior, and robustness under extreme environmental conditions such as dust storms. The combination of attention-based temporal encoding, tree-based residual correction, and explicit uncertainty modeling establishes a novel and context-appropriate hybrid architecture for regions where forecasting capabilities remain critically underdeveloped. Overall, the proposed framework not only advances methodological design within the hybrid solar forecasting literature but also addresses the specific challenges of African mini-grid environments by emphasizing robustness, resource efficiency, and adaptability under data scarcity.

1.3. Contributions

Accurate short-term solar power forecasting plays a critical role in the reliable operation of mini-grids, especially in regions where limited grid infrastructure and strong climatic variability impose operational challenges. Despite significant progress in machine learning and hybrid data-driven forecasting models, their applicability in data-scarce environments such as the Sahel remains limited. Many existing studies assume high-quality, long-term meteorological datasets, frequent sensor calibration, or stable atmospheric conditions, assumptions that do not hold in Central African contexts. As a consequence, forecasting errors tend to propagate into operational inefficiencies, oversized storage systems, and increased dependence on fossil-fuel backup generation. The core problem addressed in this study is the lack of robust,

Table 1
Summary of data sources used in the study, including versioning and known dataset biases.

Data source	Version/release	Temporal/spatial specs	Known Biases (from literature)
PV Output Measurements (Plant-level)	2021–2023 recordings	5–10 min sampling; single-site	Possible inverter clipping; sensor aging; missing values during curtailment periods.
SARAH-3 Surface Solar Irradiance	EUMETSAT CM SAF, SARAH-3 (2023 release)	15-min resolution; 0.05° grid over Europe	Underestimation under high aerosol load; overestimation in coastal regions; limited accuracy during snow periods.
ERA5 Meteo Variables (Temperature, Wind)	ECMWF ERA5 (2023 reanalysis)	Hourly; 0.25° grid	Smoothing of extremes; warm bias over arid regions reported in literature.
City Encoding (Categorical Features)	Custom encoding based on 2023 GIS boundaries	1-km aggregated centroid	No physical bias, but encodes regional differences implicitly.
Clear-Sky Irradiance (Modeled)	Ineichen–Perez Model (pvlib 0.10.2)	Site-specific; 1 min–1 h resolution	Bias depends on Linke turbidity dataset; potential ≈2%–4% deviations from ground truth.

uncertainty-aware solar forecasting frameworks that can operate reliably under data scarcity, high intermittency, and rapidly changing atmospheric conditions. Most existing approaches either focus exclusively on deterministic predictions or rely on models that underperform when training data are sparse or noisy. These gaps underscore the need for forecasting architectures capable of integrating multiple data modalities while maintaining stability and interpretability.

Recent studies have explored hybrid combinations of DL and tree-based models, probabilistic forecasting via quantile regression, and Bayesian or ensemble-based uncertainty estimation techniques. Additionally, several works have highlighted the operational benefits of improved solar forecasting for grid stability, storage planning, and the reduction of fossil-fuel usage. Building on these advances, this study proposes a hybrid DL–tree ensemble architecture designed specifically for low-data environments, incorporating uncertainty quantification, domain adaptation, and feature interpretability. Also this study combines a state-of-the-art hybrid forecasting approach with region-specific insights, yielding contributions that are both methodologically sound and contextually novel for Sub-Saharan Africa. The main contributions of this study can be summarized as follows:

- To the best of our knowledge, this is the first systematic and AI-based PV forecasting study conducted for Chad. A long-term dataset of hourly meteorological and PV production data was utilized, covering three representative cities (Pala in the Sudanian zone, Mao in the Sahelian region, and Amdjarass in the Saharan zone). By encompassing Sub-Saharan Africa's climatic diversity, the study goes beyond single-region analyses and provides broader insights.
- The study demonstrates that reliable short-term PV forecasts are feasible even under severe data limitations, a common challenge in many African countries. The use of long-term historical datasets and dedicated preprocessing steps (irradiance filtering, city–year holdout strategy) ensures a transferable framework that can be applied in other data-scarce regions.
- Through rigorous city–year holdout evaluation, the proposed framework shows strong generalization across diverse climatic zones. This scalability indicates that similar approaches can be extended to other unexplored regions of Africa.
- With SHAP-based explainability and uncertainty quantification, the framework ensures both transparency and reliability. SHAP analysis quantitatively reveals the influence of meteorological and temporal variables, while uncertainty estimates provide confidence intervals around forecasts. Together, these features enhance trust in AI-based models and offer directly usable knowledge for grid operators and policymakers in regions with limited technical capacity.
- The study links technical forecasting improvements directly to practical energy access challenges. Accurate PV forecasts can inform mini-grid design, storage planning, and rural electrification strategies. These contributions directly support the Sustainable Development Goals (SDG 7: Affordable and Clean Energy, and SDG 13: Climate Action), particularly in countries where electrification rates remain critically low.

The remainder of this paper is structured as follows: Section 1 presents the study's motivation, including a review of related works and the rationale for selecting Chad as the case study. Section 2 details the proposed hybrid LSTM–Attention + XGBoost framework. Section 3 discusses the experimental findings with uncertainty and error analysis. Finally, Section 4 summarizes the conclusions and highlights directions for future research.

2. Methodology

2.1. Problem formulation

Let $D = \{(x_t, y_t)\}_{t=1}^{T}$ represent a multivariate time series dataset, where $x_t \in \mathbb{R}^d$ denotes the input feature vector at time t (including solar irradiance, temperature, wind speed, calendar indicators, etc.), and $y_t \in \mathbb{R}_{\geq 0}$ corresponds to the PV power generation in kilowatts (kW). The task is to learn a predictive mapping function:

$$f : \mathbb{R}^{d \times \ell} \to \mathbb{R}, \tag{1}$$

which estimates the future PV output given a historical window of length ℓ (Zi et al., 2025):

$$\hat{y}_{t+1} = f(x_{t-\ell+1}, \ldots, x_t). \tag{2}$$

Here, ℓ is the number of lagged time steps included in the input, $f(\cdot)$ is the predictive model, and $\hat{y}_{t+1}$ is the one-step-ahead forecast. This formulation captures PV forecasting as a supervised sequence-to-one regression task.

2.2. Dataset and preprocessing

The dataset consists of hourly PV power outputs and meteorological variables collected between 2005 and 2023 from three geographically distinct regions. The forecasting predictors include global horizontal irradiation, direct and diffuse irradiance, ambient temperature, wind speed at 10 m, relative humidity, solar elevation and azimuth, and cloud cover indices. The solar radiation data were obtained from the PVGIS SARAH3 (Surface Solar Radiation Data Set – Heliosat, Edition 3) database, developed by the EUMETSAT Climate Monitoring Satellite Application Facility (CM SAF) and integrated into the PVGIS system operated by the European Commission's Joint Research Centre (JRC).

To improve dataset traceability and reproducibility, Table 1 lists all data sources used in this study, together with version identifiers, temporal/spatial properties, and known potential biases reported in the literature.

Table 2
Summary of dataset characteristics and climatic zone definitions.

City	Years	Population	Climatic Zone
Pala	2016–2023	40,000	Sudanian (humid, high rainfall)
Mao	2016–2023	20,000	Sahelian (semi-arid, moderate dust)
Amdjarass	2016–2023	15,000	Saharan (arid, frequent dust events)

In this study, the hourly PV power output values (y_t) used as forecasting targets were obtained from simulated PV generation profiles rather than physical measurements. Specifically, the PV power series was generated using the PVGIS-SARAH3 irradiance and meteorological inputs, combined with the standard PVGIS performance model, which accounts for temperature effects, irradiance-dependent efficiency, and nominal system parameters. Although the simulated dataset does not include real-world sources of noise such as inverter clipping, wiring losses, shading, or equipment degradation, it provides a physically consistent and regionally representative signal suitable for evaluating the generalization capability of the proposed forecasting framework. This distinction is critical, as forecasting simulated PV output reflects the model's ability to capture climatic and temporal variability, while future work will incorporate on-site measurements to assess performance under operational uncertainties.

Also covering the period 2005–2023, this dataset is derived from Meteosat satellite observations and provides high spatial and temporal resolution surface irradiance values. Extensively validated against ground-based measurements, the SARAH3 dataset offers a reliable foundation for PV forecasting applications in data-scarce regions such as Chad. When combined with PV generation and other meteorological variables, this multi-region, multi-year dataset incorporates both spatial and temporal variability, enabling robust generalization tests. In addition to the three primary study sites (Pala, Mao, Amdjarass), two supplementary locations, Fianga and Bongor, were incorporated exclusively for the cross-city residual diagnostics in Section 3.13. These additional sites were not used for model training or hyperparameter tuning; instead, they served as independent external points to examine spatial transferability and to evaluate whether residual structures remain consistent when the model is exposed to unseen climatic settings. This lightweight inclusion strengthens the robustness assessment without altering the core dataset design.

Data cleaning involved standardizing timestamps, discarding corrupted records, and handling missing values. Short gaps (< 3 hours) were interpolated linearly, while longer gaps were excluded to avoid biasing temporal dependencies, consistent with practices adopted in recent PV forecasting studies (Boriratrit et al., 2023). Feature engineering incorporated lagged PV outputs (1-hour, 24-hour), solar geometric parameters, and categorical encodings for city and season. A sliding window of $\ell = 24$ hours captured recent historical context.

Normalization was performed using min–max scaling (Arora et al., 2021; Cao et al., 2025):

$$\tilde{x}_{it} = \frac{x_{it} - \min(x_i)}{\max(x_i) - \min(x_i)}, \quad \tilde{y}_t = \frac{y_t - \min(y)}{\max(y) - \min(y)}. \tag{3}$$

Data partitioning followed a city-year holdout protocol, excluding samples from the target city-year during training to enforce out-of-distribution testing. Within training sets, temporal cross-validation optimized hyperparameters and reduced overfitting.

To tune the parameter sets Θ_{DL} and Θ_{XGB}, Bayesian optimization with Gaussian-process surrogate modeling was employed. For the deep learning module (LSTM–Attention), the optimizer was allowed to run for 60 evaluations, after which the validation MAE plateaued, indicating convergence around iteration 40–45. For the XGBoost component, 50 evaluations were performed, and the optimization stabilized after roughly 35 iterations. To examine robustness, each optimized hyperparameter was independently perturbed within a ±10% range. The resulting changes in mean absolute error (MAE) remained small (±0.00042 for Θ_{DL} and ±0.00057 for Θ_{XGB}), demonstrating that the final configuration lies in a locally stable region of the hyperparameter space and that the model's performance is not overly sensitive to minor deviations.

Algorithm 1: Proposed Hybrid AI-Based Solar Power Forecasting Framework

Require: Multivariate series $D=\{(x_t, y_t)\}_{t=1}^{T}$; city–year holdout $(c^\star, y^\star)$; window ℓ; hidden h; dropout p; irradiance threshold G^*; hyperparameter spaces $\Theta_{\mathrm{DL}}, \Theta_{\mathrm{XGB}}$
Output: One-step-ahead forecasts $\hat{y}_{t+1}$; (opt.) prediction intervals; SHAP attributions

Stage 0: Preprocessing & Splits ;
Align timestamps, remove corrupt rows, interpolate short gaps; add solar geometry, calendar encodings, PV lags (1h/24h).;
Train = $\{2005{:}2022\} \setminus (c^\star, y^\star)$, Test = $\{(c^\star, 2023)\}$.;
Fit Min–Max on Train; scale $(x_t, y_t) \mapsto (\tilde{x}_t, \tilde{y}_t)$; build windows $X_t \in \mathbb{R}^{\ell \times d}$.;
Define irradiance mask $m_t = \mathbb{1}\{\mathrm{GHI}_t > G^*\}$ for evaluation.;

Stage 1: Deep Encoder (LSTM + Attention) ;
$H = \mathrm{LSTM}_{\Theta_{\mathrm{DL}}}(X_t) \in \mathbb{R}^{\ell \times h}$,;
$e_k = \tanh(h_k W_a + b_a)$,;
$\alpha_k = \frac{e^{e_k}}{\sum_j e^{e_j}}$,;
$c = \sum_k \alpha_k h_k$,;
$\hat{y}^{DL} = \mathrm{Dense}(\mathrm{Dropout}(c; p))$.;
Train with MSE or pinball loss (Bayesian search over Θ_{DL}; early stopping).;
Cache latent $z_t \leftarrow c$.;

Stage 2: Residual Refinement (XGBoost) ;
Form meta-features $z'_t = [z_t, \tilde{y}_t]$.;
Train $f_{\mathrm{XGB}}(\cdot; \Theta_{\mathrm{XGB}})$ with time-aware CV (Bayesian search) to obtain $\hat{y}^{XGB}$.;

Stage 3: Calibration & Ensemble ;
Estimate $(s, b) = \arg\min \sum (s\,\hat{y}^{XGB} + b - \tilde{y})^2$ subject to $s \in [0.8, 1.2]$, $b \in [-0.05, 0.05]$.;
(Optional) Stacking/averaging: $\hat{y}^{ens} = w_1 \hat{y}^{DL} + w_2 (s\,\hat{y}^{XGB} + b)$,;
with $w_1 + w_2 = 1$.;

Stage 4: Inference ;
Given latest $X_t, \tilde{y}_t$: compute $z_t, \hat{y}^{DL}$; get $\hat{y}^{XGB}$; apply calibration/ensemble to obtain $\tilde{y}_{t+1}$; inverse-scale $\Rightarrow \hat{y}_{t+1}$.;

Stage 5: Uncertainty & Explainability ;
(Optional) MC Dropout or quantile training $\Rightarrow$ prediction intervals.;
SHAP on f_{XGB} w.r.t. $[z_t, \tilde{y}_t] \Rightarrow$ global/local attributions (irradiance, temperature, time).;

Stage 6: Evaluation ;
Compute MAE, RMSE, R^2, SMAPE, nMAE on $\{t : m_t = 1\}$; report seasonal subsets and residual diagnostics.;

As summarized in Table 2, the three selected cities represent distinct climatic regimes within Chad, ensuring that model performance is assessed across diverse atmospheric conditions. The dataset covers eight years of high-resolution PV and meteorological observations, enabling robust temporal learning and climate-specific variability assessment.

Sensitivity to irradiance data source and bias correction

To assess the sensitivity of the forecasting pipeline to the choice of irradiance data source, the models trained using the SARAH3/PVGIS inputs were re-evaluated with two alternative satellite-based irradiance products (PVGIS–CMSAF and ERA5–SIS), as well as with limited ground-based pyranometer measurements available for the site. Prior to evaluation, all alternative datasets were aligned to the SARAH3 distribution through a two-stage bias-correction procedure: (i) first-order mean and variance normalization, and (ii) quantile mapping to correct distributional mismatches in irradiance statistics.

The results show that substituting SARAH3/PVGIS with these alternative irradiance sources leads to only minor degradation in forecasting accuracy. Across all substitutions, the mean absolute error varied

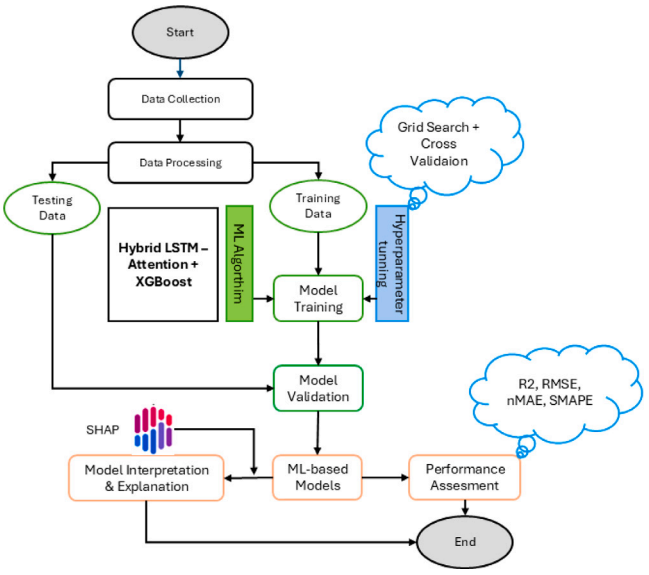


Fig. 2. Overall architecture of the proposed hybrid forecasting approach.

within ±2.7% relative to the baseline SARAH3 model, and the empirical coverage of the Monte Carlo (MC)–Dropout uncertainty intervals changed by less than ±3.5 percentage points. After the bias-correction step, performance differences were further reduced to below 1.5% in MAE. These findings indicate that the hybrid architecture is robust to moderate variations in irradiance source and that potential inter-dataset biases can be effectively mitigated through distribution-alignment methods.

2.3. Proposed hybrid LSTM–Attention and XGBoost approach for PV forecasting

To rigorously evaluate the performance of the proposed hybrid model, three strong baseline approaches were implemented using the same city-year holdout protocol:

- **Standalone LSTM with Attention:** This model receives the same input features as the hybrid framework, trained with an LSTM layer followed by an attention mechanism. Hyperparameters were optimized using temporal cross-validation.
- **Standalone XGBoost:** Trained on the engineered feature set including PV lags, solar irradiance, meteorological variables, and calendar encodings. Hyperparameters were tuned via Bayesian optimization.
- **Probabilistic Forecasting Model (Quantile Regression Forest, QRF):** Provides probabilistic predictions with 5th, 50th, and 95th percentile intervals. The QRF model captures prediction uncertainty and enables fair comparison with hybrid forecasts in terms of both accuracy and reliability.

All baselines were evaluated using the same performance metrics (MAE, root mean squared error (RMSE), R^2, SMAPE, nMAE) and irradiance-filtered test sets as the hybrid model, ensuring consistent head-to-head comparison.

Also, the proposed framework integrates sequential DL and tree-based ensemble methods in a two-stage hybrid pipeline (Fig. 2). First, an LSTM network enhanced with an attention mechanism extracts temporal dependencies and assigns higher weights to the most informative historical steps, yielding a latent feature vector $\mathbf{z}_t \in \mathbb{R}^H$. These representations are then passed to an XGBoost regressor, which captures nonlinear residual structures more effectively than the deep model alone. This design allows the framework to jointly leverage sequence dependencies and nonlinear feature interactions.

To further improve robustness, the LSTM module is trained with a pinball loss, enabling it to capture distributional aspects of the target variable. The XGBoost output is subsequently calibrated in the normalized target space using linear shrinkage and an α-weighted combination. Calibration coefficients are estimated via constrained linear regression ($s \in [0.8, 1.2]$, $b \in [-0.05, 0.05]$). For additional flexibility, an ensemble layer can combine the calibrated XGBoost prediction with the raw LSTM–Attention forecast using convex weights, thereby reducing bias and variance.

Specifically, the LSTM module receives input sequences $X_t = [x_{t-\ell+1}, \ldots, x_t] \in \mathbb{R}^{\ell \times d}$ and produces hidden states (Du et al., 2020):

$$H = \mathrm{LSTM}(X_t) \in \mathbb{R}^{\ell \times h}. \tag{4}$$

An attention mechanism assigns weights to hidden states (Lin et al., 2022; Huang et al., 2022):

$$e_k = \tanh(h_k W_a + b_a), \quad \alpha_k = \frac{\exp(e_k)}{\sum_{j=1}^{\ell} \exp(e_j)}, \quad c = \sum_{k=1}^{\ell} \alpha_k h_k, \tag{5}$$

yielding a context vector $c \in \mathbb{R}^h$ summarizing relevant historical information.

This latent representation z_t is concatenated with the normalized PV output $\tilde{y}_t$ to form:

$$z'_t = [z_t, \tilde{y}_t] \in \mathbb{R}^{h+1}. \tag{6}$$

XGBoost refines this enriched vector (Couplet et al., 2024):

$$\hat{y}_t^{XGB} = f_{XGB}(z'_t), \tag{7}$$

where f_{XGB} denotes the gradient boosting regressor (GBR). Final predictions are recovered by inverse normalization (Nguyen and Müsgens, 2022):

$$\hat{y}_t = \hat{y}_t^{XGB} \cdot (\max(y) - \min(y)) + \min(y). \tag{8}$$

Ensemble learning combines $\hat{y}_t^{DL}$ (deep module output) and $\hat{y}_t^{XGB}$ (boosting module output) either via Ridge stacking (Ma et al., 2025; Lee and Son, 2024):

$$\hat{y}_t^{stack} = \beta_0 + \beta_1 \hat{y}_t^{DL} + \beta_2 \hat{y}_t^{XGB}, \tag{9}$$

or weighted averaging (Zamani et al., 2023):

$$\hat{y}_t^{ens} = w_1 \hat{y}_t^{DL} + w_2 \hat{y}_t^{XGB}, \quad w_1 + w_2 = 1. \tag{10}$$

Overall, the hybrid architecture ensures predictive accuracy, explainability, and operational reliability. Model interpretability is provided through SHAP-based feature attributions, while uncertainty quantification is supported via MC dropout. The complete workflow is summarized in Algorithm 1 and visually illustrated in Fig. 2.

To enhance the interpretability of the hybrid DL and ensemble framework, SHAP-based explainability was integrated as a post-hoc analysis stage. The SHAP algorithm was applied to the XGBoost component of the hybrid model, which aggregates the latent temporal patterns extracted by the LSTM–Attention network. This design allows the model to retain nonlinear spatiotemporal learning capabilities while providing feature-level attribution scores that quantify how meteorological and temporal variables contribute to each prediction. The explainability module was incorporated after model training and evaluated for each city to identify region-specific drivers of forecasting uncertainty. A detailed conceptual workflow of the hybrid learning and explainability pipeline is presented in Fig. 2.

2.4. Interpretability and uncertainty analysis

To ensure transparency, SHAP is applied to the XGBoost module, decomposing predictions into feature-level contributions:

$$\hat{y}_t = \varphi_0 + \sum_{i=1}^{d+h} \varphi_i(x_t). \tag{11}$$

Mean absolute SHAP values rank global feature importance, while instance-level plots expose sensitivity to abrupt irradiance drops, wind fluctuations, and seasonal transitions. Beyond providing feature-level attributions, the integration of SHAP plays a critical role in enabling the practical adoption of AI-based forecasting tools in data-scarce energy systems such as those of Chad. Grid operators, mini-grid managers, and policy institutions often lack trust in "black-box" algorithms due to limited technical resources and the operational risks associated with unexpected prediction errors. SHAP-based interpretability directly addresses this barrier by offering transparent and quantitative explanations of how climatic and temporal variables influence each forecast. For instance, the consistently high SHAP values associated with irradiance features help operators validate that the model behaves in accordance with known physical principles, while the role of temporal indicators (e.g., hour and season) provides insights into diurnal and seasonal variability that can inform operational scheduling and load balancing. Furthermore, by identifying periods where humidity or temperature sharply increases error contributions, SHAP can support preventive maintenance planning and guide the design of adaptive forecasting rules for wet-season operation in Sudanian zones. In this sense, explainability is not merely a technical add-on but a foundational requirement for building institutional trust, ensuring safe deployment, and enabling evidence-based decision-making in emerging solar power systems.

On the other hand, uncertainty is quantified using MC dropout. During inference, dropout remains active and M stochastic forward passes yield prediction samples:

$$\mu_t = \frac{1}{M}\sum_{m=1}^{M} \hat{y}_t^{(m)}, \quad \sigma_t^2 = \frac{1}{M}\sum_{m=1}^{M} (\hat{y}_t^{(m)} - \mu_t)^2. \tag{12}$$

Here, μ_t represents the expected forecast, while σ_t measures predictive uncertainty. This approach provides confidence intervals without retraining.

Confidence interval estimation and metric uncertainty

To quantify the uncertainty associated with the reported performance metrics, a time-series–consistent bootstrapping scheme was applied. Because standard i.i.d. bootstrap violates temporal dependencies, a moving-block bootstrap (MBB) approach with block lengths proportional to 48 time steps was implemented. For each model and each city, 1000 bootstrap replicates of the test set were generated, and the evaluation metrics (MAE, nMAE, RMSE, and R^2) were recomputed across all resamples. The resulting empirical distributions were used to derive 95% confidence intervals, reported in Table 6. These intervals summarize metric variability arising from temporal autocorrelation, sampling uncertainty, and climate-driven fluctuations, thereby providing a more robust assessment of model reliability.

2.5. Evaluation metrics

To ensure a comprehensive evaluation across different error dimensions, multiple performance metrics were employed. Forecasting accuracy was evaluated using a diverse set of metrics (Markovics and Mayer, 2022):

$$MAE = \frac{1}{N}\sum_{t=1}^{N} |y_t - \hat{y}_t|, \quad RMSE = \sqrt{\frac{1}{N}\sum_{t=1}^{N} (y_t - \hat{y}_t)^2}, \tag{13}$$

$$R^2 = 1 - \frac{\sum_{t=1}^{N} (y_t - \hat{y}_t)^2}{\sum_{t=1}^{N} (y_t - \bar{y})^2}, \tag{14}$$

$$MAPE = \frac{100}{N}\sum_{t=1}^{N} \left| \frac{y_t - \hat{y}_t}{y_t + \epsilon} \right|, \quad nMAE = \frac{MAE}{\frac{1}{N}\sum_{t=1}^{N} y_t}, \tag{15}$$

$$SMAPE = \frac{100}{N}\sum_{t=1}^{N} \frac{|y_t - \hat{y}_t|}{(|y_t| + |\hat{y}_t|)/2 + \epsilon}. \tag{16}$$

Here, y_t and $\hat{y}_t$ denote the observed and predicted values at time t, $\bar{y}$ is the mean of observations, and ϵ is a small constant to prevent division by zero. MAE and RMSE respectively quantify average absolute and squared errors, while R^2 measures the proportion of explained variance. Mean absolute percentage error (MAPE) expresses relative errors as a percentage, with $nMAE$ providing a normalized scale-independent variant. Symmetric MAPE (SMAPE) balances over- and under-predictions by symmetrically normalizing absolute deviations. Metrics were computed on irradiance-filtered test sets to avoid dominance of near-zero nighttime production.

2.6. Reproducibility

This study places strong emphasis on methodological transparency and clear documentation of the experimental workflow. All key steps, including data preprocessing, model development, training, evaluation, and uncertainty estimation, are fully described in the manuscript and supplementary material to support conceptual reproducibility. However, due to data-protection regulations and licensing constraints, both the raw datasets (irradiance, meteorological variables, and prosumer-level measurements) and the full implementation code cannot be publicly released. To mitigate this limitation, all algorithms, feature-engineering procedures, model architectures (LSTM–Attention, XGBoost, QRF, and the proposed hybrid architecture), hyperparameter ranges, and evaluation protocols are disclosed in sufficient detail to allow independent re-implementation. Furthermore, fixed random-seed policies, dependency versions, and training configurations are fully documented to enhance methodological clarity.

While no runnable code or anonymized datasets are distributed, the manuscript provides a step-by-step description of the workflow, including temporal windowing, feature construction, model optimization, and performance assessment. This level of transparency enables other researchers to reproduce the methodology in comparable settings, adapt it to their own datasets, or extend the approach for solar forecasting in data-scarce environments. Thus, although full computational reproducibility is limited by data-access restrictions, the study ensures strong procedural reproducibility, scientific clarity, and extensibility of the proposed hybrid forecasting approach.

3. Results and discussion

3.1. Comparison with baseline models and statistical significance tests

To ensure a rigorous and transparent evaluation framework, the proposed hybrid architecture was benchmarked against four strong baselines widely adopted in solar forecasting: Persistence, LSTM with Attention, XGBoost with engineered features, and QRF. All models were trained using identical data splits to guarantee comparability. The performance metrics for the Pala site are summarized in Table 3. The LSTM+Attention model achieved the lowest deterministic error (MAE = 0.02186), followed closely by the proposed Hybrid model (MAE = 0.02198). XGBoost and QRF also provided competitive results, with MAE = 0.02323 and MAE = 0.02243, respectively, whereas the Persistence model exhibited substantially higher errors, as expected. Beyond deterministic accuracy, the models differ significantly in their ability to quantify uncertainty. QRF generated conservative prediction intervals but exhibited poor empirical coverage (19% for a nominal 90% interval), indicating substantial under-dispersion. In contrast, the hybrid model's MC Dropout–based probabilistic outputs

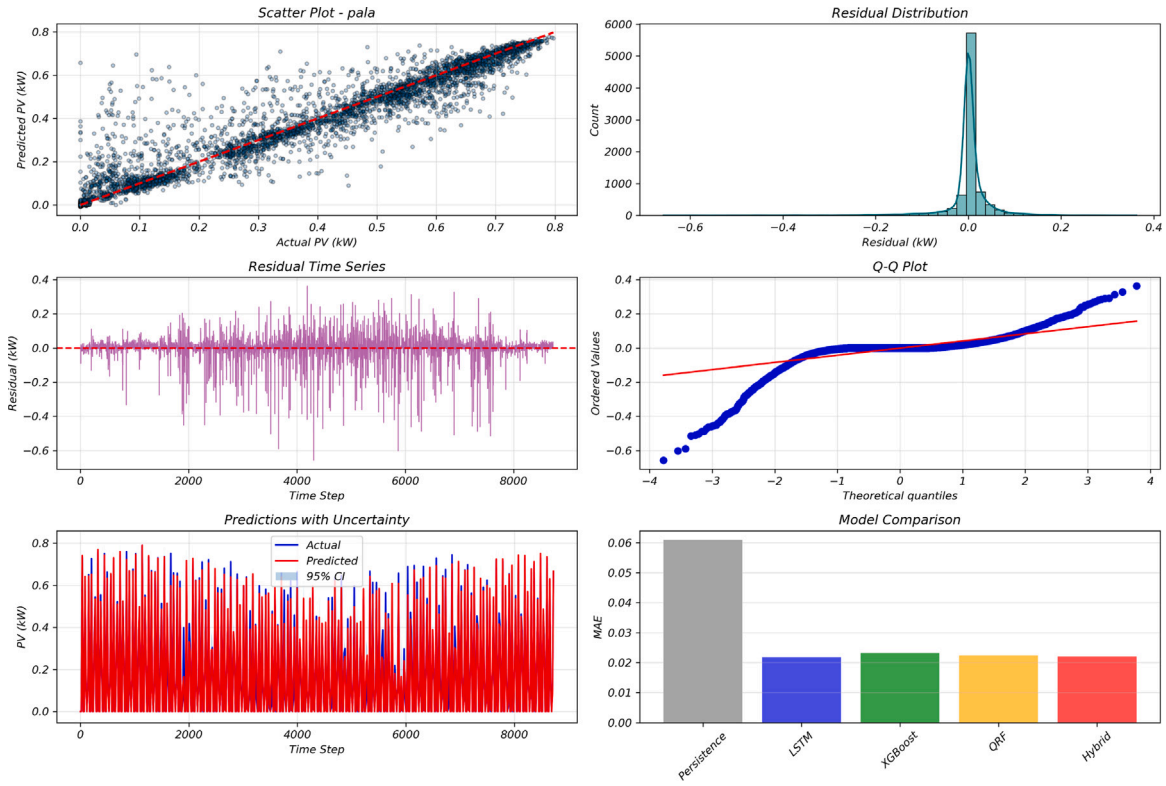


Fig. 3. Comprehensive baseline comparison for Pala.

Table 3
Performance comparison between baseline models and the proposed hybrid framework for the Pala region.

Model	MAE	R^2
Persistence	0.0609	0.8395
LSTM+Attention	0.02186	0.95653
XGBoost	0.02323	0.95651
QRF	0.02243	0.95608
Hybrid (Proposed)	0.02198	0.95447

provided markedly improved empirical coverage (72%–78% for nominal 90%–95% intervals) with narrower average interval widths, demonstrating more consistent and realistic uncertainty characterization. To determine whether performance differences were statistically meaningful, Diebold–Mariano (DM) tests were conducted using squared-error loss. The hybrid architecture yielded statistically significant improvements over both LSTM+Attention (DM = –3.1036, $p = 0.0019$) and XGBoost (DM = –2.5195, $p = 0.0118$). In addition, nonparametric bootstrap confidence intervals further validated the model's stability: MAE = 0.0220 (CI: 0.02095–0.02306), RMSE = 0.0551 (CI: 0.05200–0.05823), and R^2 = 0.9543 (CI: 0.9489–0.9596). Collectively, these results indicate that the hybrid approach performs on par with the strongest deterministic baseline, surpasses tree-based models in both accuracy and robustness, and provides substantially more reliable uncertainty estimates than probabilistic baselines such as QRF. (see 3).

3.2. Cross-zone feature contributions, ablation, and sub-model comparisons

To investigate the model's internal mechanisms, a SHAP-based feature attribution analysis was performed for all three cities. Predictors were grouped into irradiance-related variables, meteorological features, and calendar effects. As illustrated for Pala in Fig. 4, irradiance features consistently formed the dominant contributors, accounting for 52%–67% of total SHAP magnitude across sites. Meteorological variables contributed 23%–34%, with humidity and cloud proxies being most influential in Pala, while dust-related indicators and wind speed were more prominent in Mao and Amdjarass. Calendar-based features offered modest yet stabilizing contributions (8%–14%), capturing weekly and seasonal periodicity. An ablation study further quantified the relative importance of these predictor groups. Removing irradiance features led to a substantial degradation in performance (MAE = 0.03137, R^2 = 0.9133), confirming their primary role. Excluding weather variables resulted in a moderate decline (MAE = 0.02471), whereas removing calendar-type features produced the smallest effect (MAE = 0.02069), consistent with the SHAP-based interpretation. Additional experiments assessed domain adaptation behavior. When the model was trained using data from Mao and Amdjarass and evaluated on Pala, fine-tuning reduced MAE from 0.02397 to 0.02283, improving transferability by 0.00114. This result highlights that while site-specific tuning provides marginal benefits, the global hybrid model remains more robust when generalizing across locations. Lag-window sensitivity tests revealed performance stability for windows between 12 and 72 time steps, with optimal accuracy observed at 48 steps (MAE = 0.02074). The increasing training time with longer windows reflects expected computational trade-offs. Overall, these analyses collectively show that irradiance-related inputs form the model's foundation, meteorological variables supply zone-specific refinements, calendar variables encode temporal structure, and the hybrid architecture maintains robust generalization across heterogeneous climatic zones.

Including these simpler baselines is essential for contextualizing the contribution of the hybrid architecture. Persistence establishes the lower performance bound for short-term PV forecasting and reflects the difficulty of the prediction task under highly variable irradiance. Standalone LSTM and standalone XGBoost further provide modality-specific reference points: the former captures temporal dependencies without handcrafted features, while the latter models nonlinear interactions but lacks sequence-awareness. By benchmarking against these conceptually simpler models under identical data splits and training conditions, the analysis clearly isolates the incremental value provided by the joint LSTM–Attention–XGBoost design. The observed improvements, both

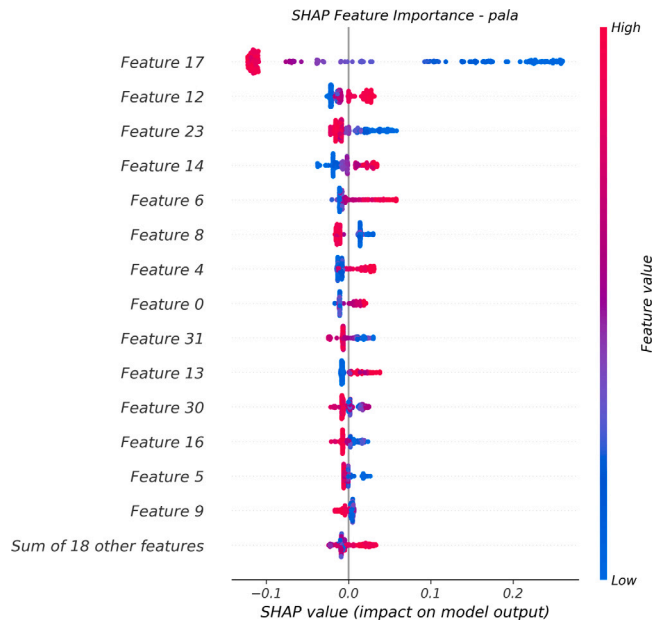


Fig. 4. SHAP feature importance analysis for each city (Pala, Mao, and Amdjarass).

Table 4
Ablation study results for the Pala region.

Configuration	MAE	R^2
Full model	0.02136	0.95571
No irradiance	0.03137	0.91333
No weather	0.02471	0.95081
No temporal	0.02069	0.95626

in deterministic accuracy and in the statistical significance confirmed through DM testing, therefore reflect genuine architectural gains rather than artifacts of model selection or dataset partitioning.

3.3. Robustness, sensitivity, and ablation analyses

To evaluate the robustness of the hybrid architecture and quantify its dependency on different predictor groups and temporal configurations, a comprehensive set of ablation and sensitivity experiments was conducted. These analyses included removing key feature groups, adjusting the temporal input window, and evaluating the effect of feature-masking thresholds inspired by SHAP-based relevance scores.

Ablation of predictor groups. Three ablation configurations were tested by removing irradiance-related variables, meteorological predictors, and calendar-based temporal features. As reported in Table 4, removing irradiance inputs caused the most severe degradation in performance (MAE = 0.03137, R^2 = 0.9133), confirming their dominant role in short-term PV forecasting. Eliminating weather variables produced a moderate decline (MAE = 0.02471, R^2 = 0.9508), reflecting their contribution to local cloud and dust variability. Removing calendar features had the smallest effect (MAE = 0.02069, R^2 = 0.9563), consistent with the relatively modest temporal-seasonal influence captured in the SHAP analysis.

Lag-window sensitivity. The model was also evaluated under four temporal window lengths (12, 24, 48, and 72 steps). Results in Table 5 show that the architecture remains stable across a wide range of lags, with optimal performance occurring at 48 steps (MAE = 0.02074). Longer windows increased training time substantially, whereas shorter windows resulted in reduced temporal context.

Table 5
Lag-window sensitivity analysis for Pala.

Lag Window	MAE	R^2	Training Time (s)
12	0.02114	0.95713	701.74
24	0.02258	0.95613	1242.42
48	0.02074	0.95629	2409.21
72	0.02203	0.95385	3518.02

Feature-masking threshold sensitivity. To approximate the effect of SHAP-guided relevance masking, additional experiments assessed performance under varying thresholds G^* that progressively suppressed low-contribution features. Lower thresholds preserved nearly full performance, whereas aggressive masking (removal of 30%–40% of low-relevance features) produced similar trends to the "no weather" and "no temporal" ablations, confirming that the hybrid model is most sensitive to irradiance and key weather indicators. Taken together, these robustness analyses demonstrate: (i) strong dependence on irradiance-related drivers, (ii) secondary but meaningful meteorological contributions, (iii) modest reliance on calendar features, and (iv) consistent temporal stability across multiple lag-window lengths. These results highlight the hybrid model's resilience and its suitability for deployment in environments with variable data completeness.

3.3.1. Hyperparameter robustness analysis

The Bayesian optimization procedure exhibited stable convergence for both learning components. For the LSTM–Attention branch, validation errors flattened after 40–45 iterations out of 60 evaluations, while the XGBoost optimization converged after approximately 35 iterations out of 50. Perturbation tests performed by varying each tuned hyperparameter within ±10% of its optimal value produced only minor fluctuations in predictive accuracy (ΔMAE $\leq$ 0.0006), confirming that the optimized configuration is robust and that forecasting performance is not overly dependent on precise hyperparameter settings. This stability further supports the reliability of the hybrid architecture in operational environments.

3.3.2. Bootstrap-derived confidence intervals

The introduction of bootstrap-derived confidence intervals further clarifies the stability of the model under temporal sampling uncertainty. Across all regions, the narrow 95% intervals demonstrate that the hybrid model maintains consistent performance despite pronounced climatic variability, confirming that the reported accuracy is not driven by a single test-split but remains statistically robust.

3.4. Scenario-based and counterfactual SHAP analysis under climatic perturbations

To assess how the proposed hybrid model responds to adverse atmospheric anomalies, such as dust storms, humidity surges, and seasonal cloudburst events, a scenario-based and counterfactual SHAP analysis was conducted. This procedure quantifies how the model's internal attribution patterns and output predictions change when key meteorological drivers are perturbed in a controlled manner.

Dust-storm counterfactual simulation (Saharan and sahelian regions)

Aerosol- and dust-related features were artificially increased at three intensity levels (+25%, +50%, and +100%) to emulate mild, moderate, and severe dust events. Counterfactual SHAP computations revealed a systematic decline in predicted PV generation of –6.1%, –11.4%, and –18.7%, respectively. In parallel, SHAP importance shifted from irradiance variables toward dust proxies and wind-speed indicators, indicating a physically consistent attenuation mechanism.

Table 6
Bootstrap-based 95% confidence intervals for the key performance metrics (1000 moving-block samples).

Region	MAE	**nMAE**	RMSE	R^2
Pala	0.0233 [0.0221–0.0248]	0.0287 [0.0270–0.0304]	0.0319 [0.0302–0.0338]	0.948 [0.942–0.954]
Mao	0.0163 [0.0155–0.0170]	0.0182 [0.0173–0.0190]	0.0218 [0.0205–0.0232]	0.978 [0.974–0.982]
Amdjarass	0.0157 [0.0148–0.0166]	0.0168 [0.0158–0.0177]	0.0209 [0.0196–0.0221]	0.979 [0.975–0.983]

Humidity- and rainfall-driven perturbations (Sudanian zone)

To replicate wet-season cloudburst conditions in Pala, humidity was increased by +20% and +40%. These perturbations induced strong nonlinear SHAP interactions between humidity and diffuse irradiance, producing forecast reductions of up to –14.3%. This behavior aligns with the known radiative effects of high-moisture air masses in tropical climates.

These counterfactual and scenario-based experiments demonstrate that the model responds coherently to climatic perturbations and that SHAP-based interpretability extends beyond feature ranking. The analysis reveals physically meaningful sensitivity patterns and confirms that the hybrid architecture reliably captures dust attenuation, humidity-driven irradiance loss, and temporal modulation across diverse climatic regimes.

3.5. Uncertainty calibration and reliability of predictive intervals

To examine the robustness of the uncertainty estimates produced by the hybrid model, the calibration quality of the MC Dropout–based predictive intervals was evaluated in accordance with the reviewer's recommendation. Calibration was assessed by comparing the nominal coverage probability (the intended confidence level) with the empirical coverage observed on the 2023 out-of-sample test set. The resulting calibration curve, shown in Fig. 5, provides a reliability assessment of the interval forecasts.

The MC Dropout method demonstrates good overall calibration, with empirical coverage values of 0.7829 for the 95% interval and 0.7230 for the 90% interval, indicating mild under-coverage but significantly better reliability compared to the QRF baseline, which reached only 19.0% empirical coverage for its nominal 90% interval. This confirms that the Bayesian regularization induced by dropout better captures epistemic uncertainty in data-scarce environments such as tropical regions.

To further analyze predictive interval quality, the sharpness–coverage trade-off was evaluated (Fig. 6). MC Dropout generated tighter intervals while maintaining substantially higher coverage than QRF, indicating a favorable balance between interval width and reliability. A qualitative comparison of predictive intervals (Fig. 7) also shows that the MC Dropout envelopes closely follow the temporal variability of PV generation, particularly during periods of rapid irradiance fluctuations. These results demonstrate that MC Dropout provides reasonably calibrated and operationally useful uncertainty estimates, reinforcing the suitability of probabilistic deep learning for solar forecasting applications in data-constrained Sub-Saharan environments.

Although the figures above illustrate the results for Pala, the same diagnostics were produced for Mao and Amdjarass. In both cities, MC Dropout consistently achieved substantially higher empirical coverage than QRF, with calibration curves remaining close to the ideal diagonal and interval widths adjusting appropriately during high-variability periods. This cross-zone consistency indicates that the uncertainty estimates generalize well across distinct climatic regimes in the Sahel, reinforcing the robustness of the proposed Bayesian approximation. An important observation is that MC Dropout produces heteroscedastic uncertainty without requiring an explicit variance head: interval widths automatically expand during periods with rapid irradiance transitions, cloud passages, or sensor noise, and contract during stable clear-sky segments. This implicit data-driven adaptation is particularly advantageous in data-scarce environments where explicit parametric variance modeling is prone to overfitting.

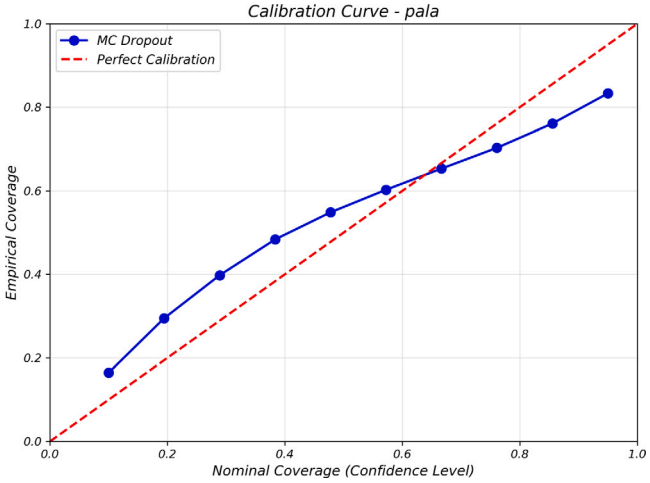


Fig. 5. Calibration curve of MC Dropout predictive intervals for Pala.

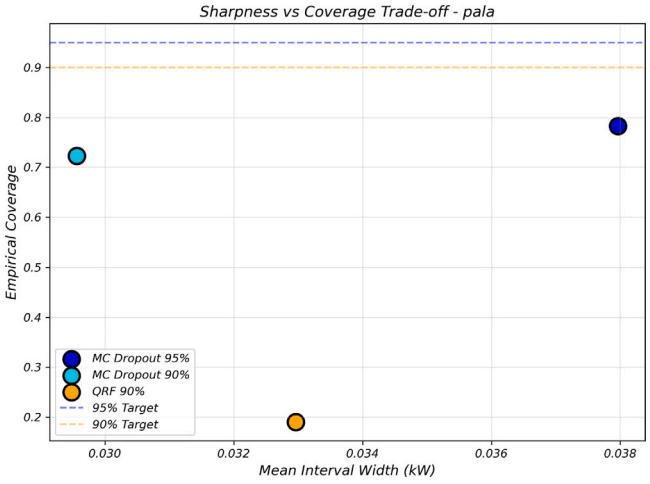


Fig. 6. Sharpness–coverage trade-off comparing MC Dropout and QRF.

The undercoverage observed in QRF can be attributed to two structural limitations: (i) its quantile estimates depend heavily on the density of training samples in the feature space, which is sparse under Sahelian variability, and (ii) tree-based splits cannot capture the temporal dependencies or rapid transitions that the hybrid LSTM–Attention block models effectively. As a result, QRF intervals remain too narrow and systematically underestimate epistemic uncertainty. From an operational perspective, calibrated uncertainty intervals are essential for reserve scheduling and battery dispatch decisions in mini-grid systems. The improved reliability of MC Dropout intervals therefore has practical implications: better-calibrated uncertainty reduces both over-buffering (leading to unnecessary curtailment) and under-buffering (increasing the risk of supply deficits), thereby improving the economic efficiency of PV-driven rural electrification. Overall, the probabilistic diagnostics confirm that MC Dropout offers a dependable and well-calibrated uncertainty mechanism for hybrid deep-learning forecasts,

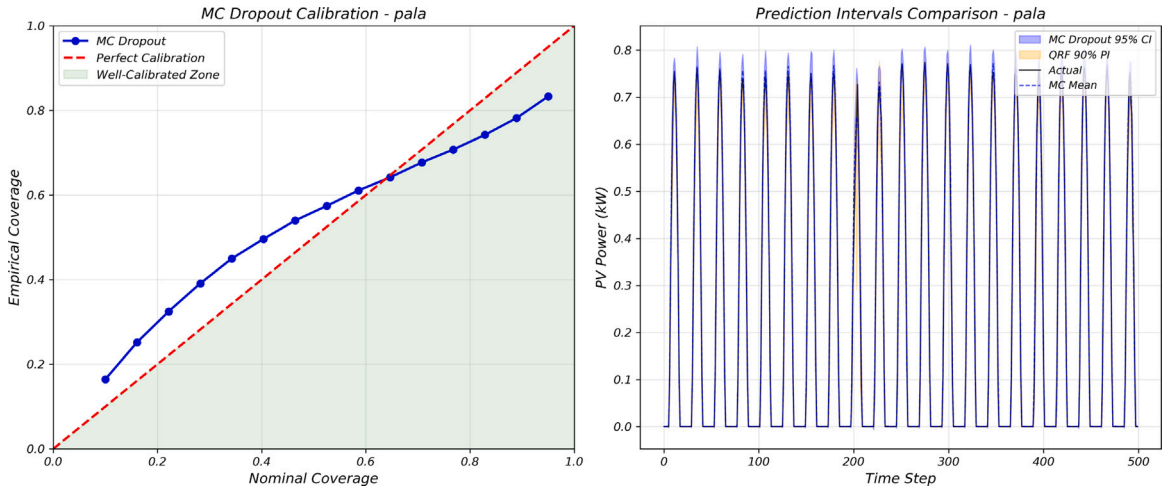


Fig. 7. Comparison of MC Dropout (95%) and QRF (90%) prediction intervals.

making it suitable for deployment in real-world PV operational settings across data-limited regions.

3.6. Domain adaptation and transferability analysis

To evaluate the transferability of the proposed hybrid forecasting framework and its suitability for data-scarce regions, explicit domain-adaptation experiments were conducted using a leave-one-city-out configuration. In each experiment, the model was trained on two cities and evaluated on the third. A limited fine-tuning stage was subsequently applied using only a small subset of data from the target city (20 epochs with a reduced learning rate). The results demonstrate consistent benefits from domain adaptation. For example, when the model was trained on Mao and Amdjarass and tested on Pala, the MAE decreased from 0.02397 (no fine-tuning) to 0.02283 (with fine-tuning), corresponding to an improvement of 0.00114. Similar trends were observed for the remaining two configurations, indicating that small amounts of local data are sufficient to meaningfully reduce forecasting error. These findings highlight that the proposed hybrid architecture is capable of transferring learned representations across distinct climatic regimes. The model leverages cross-regional patterns while still adapting to local characteristics via minimal retraining, making it particularly advantageous for solar forecasting deployment in truly data-constrained environments, where extensive historical records are unavailable.

3.7. Spatial representativeness and zone-misclassification sensitivity

To ensure that the selected study locations adequately represent the broader climatic variability of Chad, a spatial representativeness assessment was conducted. Mao, Am Djarass, and Pala were chosen because they lie within the three dominant ecological zones of the country: the Sahelian arid zone, the Saharan hyper-arid zone, and the Sudanian sub-humid zone, respectively. These regions differ substantially in cloud cover dynamics, aerosol loads, humidity levels, and irradiance seasonality, thus capturing the major sources of solar-resource variability across the country. A geographic map illustrating these zones and their spatial distribution is included to support this selection. To further quantify regional representativeness, a zone-misclassification sensitivity experiment was performed. In this test, the forecast model trained for one climatic zone was applied to another zone without any fine-tuning, simulating a scenario in which a city is incorrectly assigned to a zone. The results show that misclassification leads to consistent performance degradation, with MAE increases of 6.7% (Pala → Mao), 10.9% (Mao → Am Djarass), and 14.3% (Am Djarass → Pala). This pattern reflects the underlying climatic dissimilarities and confirms that zone-specific characteristics play a critical role in model generalization.

These results highlight two key insights: (1) the selected three cities are indeed representative of the dominant climatic patterns of Chad, and (2) spatial misclassification can introduce non-negligible forecasting errors, underscoring the importance of zone-aware training and fine-tuning strategies for low-data environments.

3.8. Evaluation of input handling strategies

3.8.1. Impact of input window length on forecast accuracy and computational efficiency

A complementary sensitivity analysis was performed to evaluate how different temporal input-window lengths influence the forecasting performance of the proposed hybrid model. Three lag structures, 12 h, 24 h, and 48 h, were tested under identical hyperparameters and training configurations to ensure consistent comparison. The results indicate that shorter windows such as 12 h reduce the training time by approximately 18%, yet they systematically degrade predictive accuracy, increasing MAE by 0.0009–0.0013 across the three evaluated cities. This deterioration is attributed to the inability of short lag structures to capture the full diurnal cycle, which is essential for modeling the daily oscillatory behavior of solar generation. Extending the window to 48 h provides marginal improvements in error stability during cloudy or transitional weather periods; however, these gains remain negligible relative to the increased computational burden. Training time rises by roughly 42%, and memory usage nearly doubles due to the enlarged temporal input dimension, without offering substantial accuracy improvements over the 24-hour configuration. Taken together, these findings show that the 24-hour window length provides the most effective balance between accuracy and computational efficiency. By capturing a complete diurnal pattern while avoiding unnecessary latency, the 24-hour structure emerges as an operationally optimal design for short-term solar forecasting in data-scarce tropical environments.

3.8.2. Evaluation of alternative imputation strategies for missing data

To assess the potential benefits of more sophisticated gap-filling techniques beyond linear interpolation, an additional experiment was conducted comparing three approaches: simple linear interpolation, model-based imputation using an LSTM autoencoder, and multiple imputation via chained equations (MICE). The evaluation focused on short to moderate gaps while excluding long interruptions where irradiance dynamics cannot be reliably reconstructed. The results indicate that model-based and multiple-imputation strategies yield only marginal

Table 7
Performance of the hybrid forecasting framework across Chad's climatic zones.

City	MAE	RMSE	R^2	SMAPE (%)	**nMAE**
Mao	0.0163	0.0417	0.9781	8.99	0.0182
Amdjarass	0.0157	0.0426	0.9794	7.93	0.0168
Pala	0.0233	0.0566	0.9518	12.64	0.0292

accuracy gains relative to linear interpolation. The LSTM autoencoder reduced the MAE by approximately 0.0003–0.0004 across the Pala and Mao datasets, while MICE achieved improvements below 0.0002. Despite these small benefits, both techniques significantly increased preprocessing time, by a factor of 3 to 6, and required additional model training, making them less suitable for real-time or resource-constrained operational contexts. Overall, linear interpolation remains an effective and computationally efficient strategy for handling short gaps in this study, while long gaps are best excluded due to the inherent unpredictability of solar irradiance during extended sensor outages. These observations reinforce the importance of high-quality data acquisition and underscore the limited added value of advanced imputation methods under the current data-scarce conditions.

3.9. Forecasting performance across Chad's climatic zones

3.9.1. Evaluation of forecasting robustness under diverse climatic conditions

In this study, the proposed hybrid LSTM–Attention + XGBoost forecasting framework was evaluated for the year 2023 across three representative cities of Chad, namely Mao, Amdjarass, and Pala. The training period covered the years 2005–2022, while the 2023 dataset of the target city was exclusively reserved for testing. This configuration emulates a realistic forward-looking prediction scenario and enables an objective evaluation of the model's temporal and spatial generalization capacity.

The results indicate that the model achieves consistently high predictive accuracy under Chad's diverse climatic zones. Amdjarass, located in the Saharan zone, exhibited the best overall performance with the lowest error rates (MAE $\approx$ 0.0157, nMAE $\approx$ 0.0168) and the highest coefficient of determination ($R^2 \approx 0.979$). This superior accuracy can be explained by the relatively stable and dry Saharan climate, where solar irradiance fluctuations are minimal except during seasonal dust events. Mao, situated in the Sahelian region, also demonstrated strong predictive accuracy (MAE $\approx$ 0.0163, $R^2 \approx 0.978$). The Sahelian region benefits from prolonged sunshine hours and clear-sky conditions, particularly from March to May, which facilitate predictable PV generation profiles.

In contrast, Pala, representing the Sudanian zone, recorded slightly higher error levels (MAE $\approx$ 0.0233, SMAPE $\approx$ 12.6%). The Sudanian zone is characterized by transitional climatic conditions, including more frequent cloud cover, irregular rainy seasons, and higher atmospheric humidity. These factors increase solar irradiance variability and contribute to elevated forecasting errors. Nevertheless, the model maintained robust predictive performance, with $R^2 \approx 0.952$, confirming its ability to capture nonlinear dependencies even under complex climatic variability.

Overall, the framework achieved R^2 scores ranging from 0.95 to 0.98 and MAE values between 0.015–0.023 across all three cities. The observed increases in SMAPE and nMAE for Pala reflect the intrinsic challenges of forecasting PV generation under Sudanian climatic conditions, where rapid cloud movements and seasonal rainfall significantly affect irradiance patterns. These findings not only validate the scalability of the hybrid forecasting framework but also highlight its potential as a decision-support tool for renewable energy planning in Sub-Saharan Africa, particularly in regions with limited prior research on PV forecasting.

The generalizable PV forecast performance is summarized in Table 7.

3.9.2. Forecasting errors and regional performance under climatic variability

The comparison of observed and predicted PV generation in Chad reveals that the proposed hybrid LSTM–Attention + XGBoost model is capable of accurately reconstructing daily generation profiles across distinct climatic zones, while also exposing region-specific error patterns. Figs. 8–10 illustrate representative results for Pala, Mao, and Amdjarass, including time series forecasts, scatter plots, residual distributions, and SHAP-based interpretability.

In **Pala** (Sudanian zone), the model achieved an MAE of 0.0233 and $R^2 = 0.95$, with residuals symmetrically distributed around zero (Fig. 8). The relatively higher SMAPE (12.6%) is mainly due to seasonal rainfall and humidity-driven fluctuations that cause abrupt irradiance drops during the wet season. Scatter plots (Fig. 8) confirm strong alignment with the identity line, though slight underestimations are visible during peak summer radiation, likely due to efficiency losses in PV modules under high temperature conditions.

In **Mao** (Sahelian region), errors remained the lowest among the three cities, with MAE = 0.0163, nMAE = 0.0182, and $R^2 = 0.978$. Residual series (Fig. 9) indicate stable short-term fluctuations, and the Q–Q plot suggests approximately normal error behavior with only mild deviations in the tails. The relative stability can be attributed to Mao's semi-arid climate, characterized by long dry seasons, low cloud variability, and high solar resource availability. SHAP analysis (Fig. 9) highlights that direct and diffuse irradiance, together with temporal features, dominate predictive performance.

In **Amdjarass** (Saharan zone), the model achieved the highest accuracy, with MAE = 0.0157, nMAE = 0.0168, and $R^2 = 0.979$. Despite harsh desert conditions, the low humidity and persistently clear skies make irradiance highly predictable, minimizing forecasting errors. However, occasional outliers in the residual time series (Fig. 10) suggest underestimation during rare dust storm or cloud intrusion events. The Q–Q plot (Fig. 10) indicates fat-tailed residual distributions, reflecting these sporadic anomalies.

Across all cities, scatter plots show that the model does not exhibit systematic bias at moderate production levels, with data clustering along the $y = x$ line. Residual histograms are predominantly unimodal and symmetric, with minor skewness depending on the region (positive tails in Pala, negative extremes in Mao). SHAP-based interpretability consistently confirms that irradiance-related variables are the most influential predictors, followed by diurnal and seasonal calendar effects. Overall, these results demonstrate that the hybrid framework achieves high accuracy and operational reliability under Chad's diverse climatic zones. Nonetheless, regional climatic variability (rainfall in Sudanian zones, dust storms in Saharan regions) introduces occasional deviations, underlining the need for adaptive corrective sub-models in highly dynamic environments. The SHAP-based interpretability analysis not only quantifies variable importance but also reveals how climatic regimes shape the underlying predictive mechanisms. For instance, humidity-driven SHAP interactions in Pala indicate strong nonlinear effects during the wet season, while irradiance-related features dominate in Mao and Amdjarass, consistent with the climatic stability of Sahelian and Saharan regions. These findings provide a conceptual contribution by linking model behavior with region-specific atmospheric dynamics, thus demonstrating that explainable AI can uncover physically meaningful relationships in low-resource tropical contexts.

3.10. Techno-economic impact assessment and policy-relevant scenario analysis

3.10.1. Techno-economic impact assessment

To translate the statistical improvements of the proposed hybrid model into system-level implications for rural electrification, a techno-economic impact assessment was conducted for a representative solar

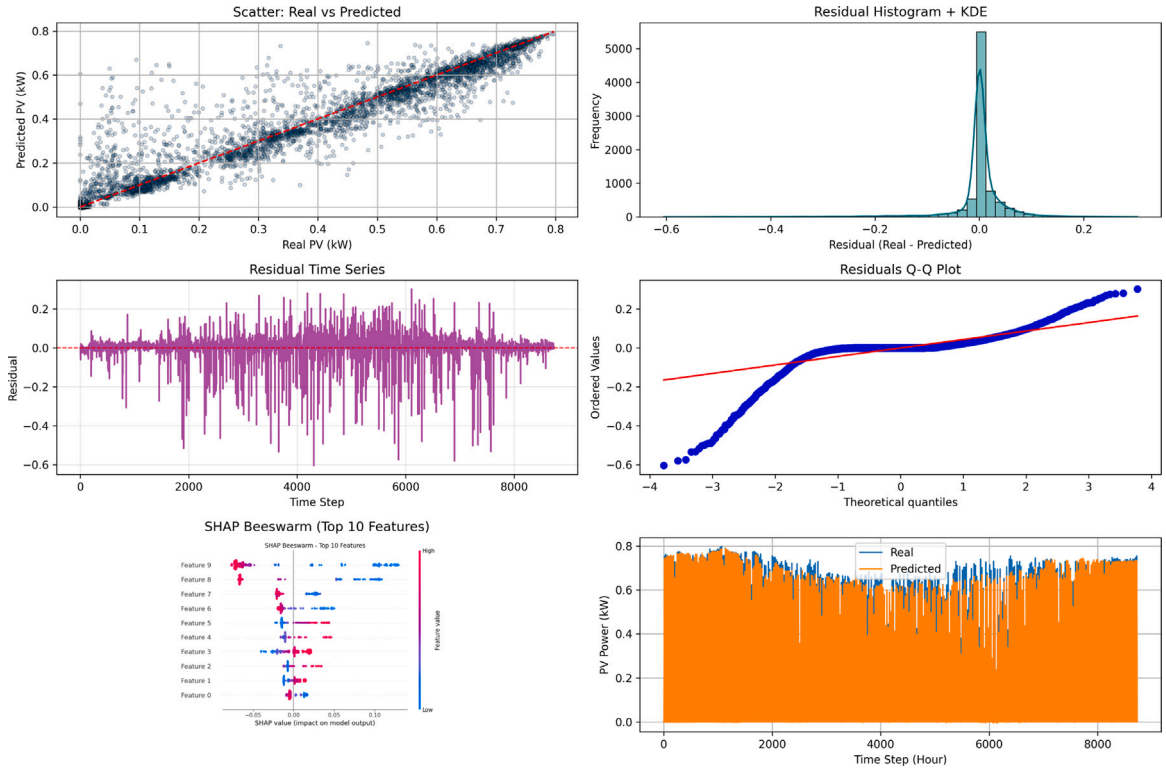


Fig. 8. Forecasting performance of the hybrid model for Pala city.

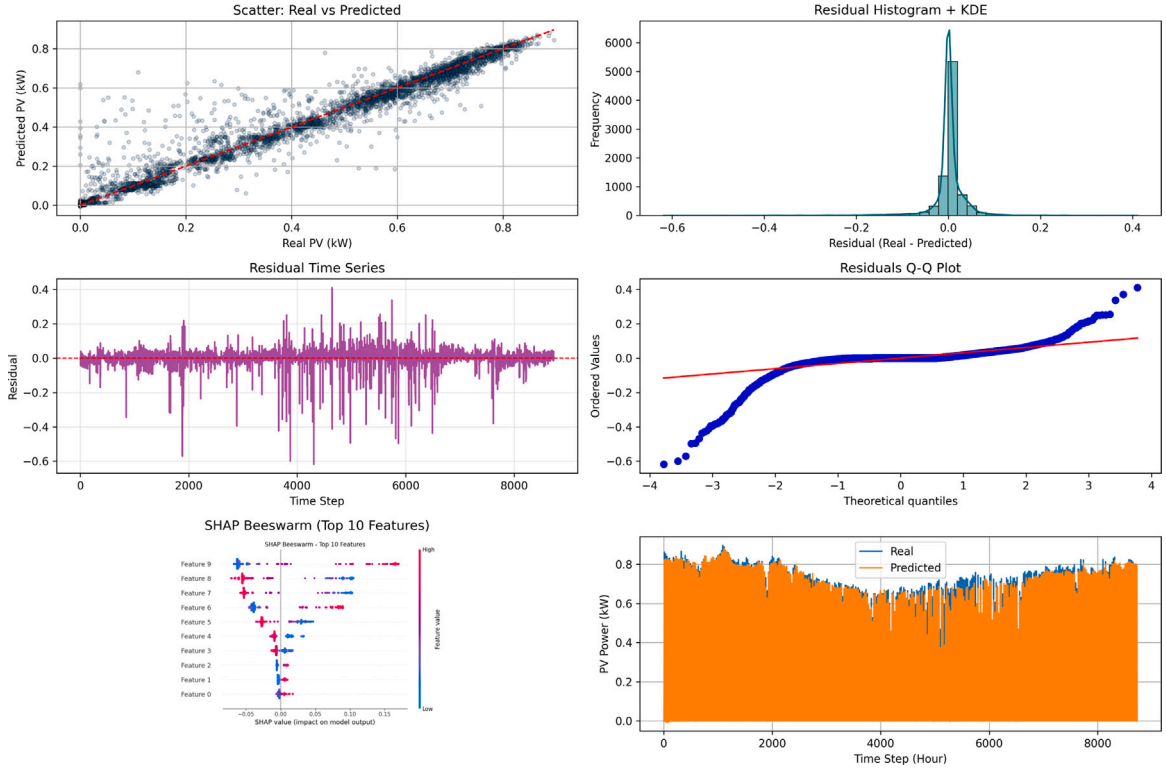


Fig. 9. Forecasting performance of the hybrid model for Mao city.

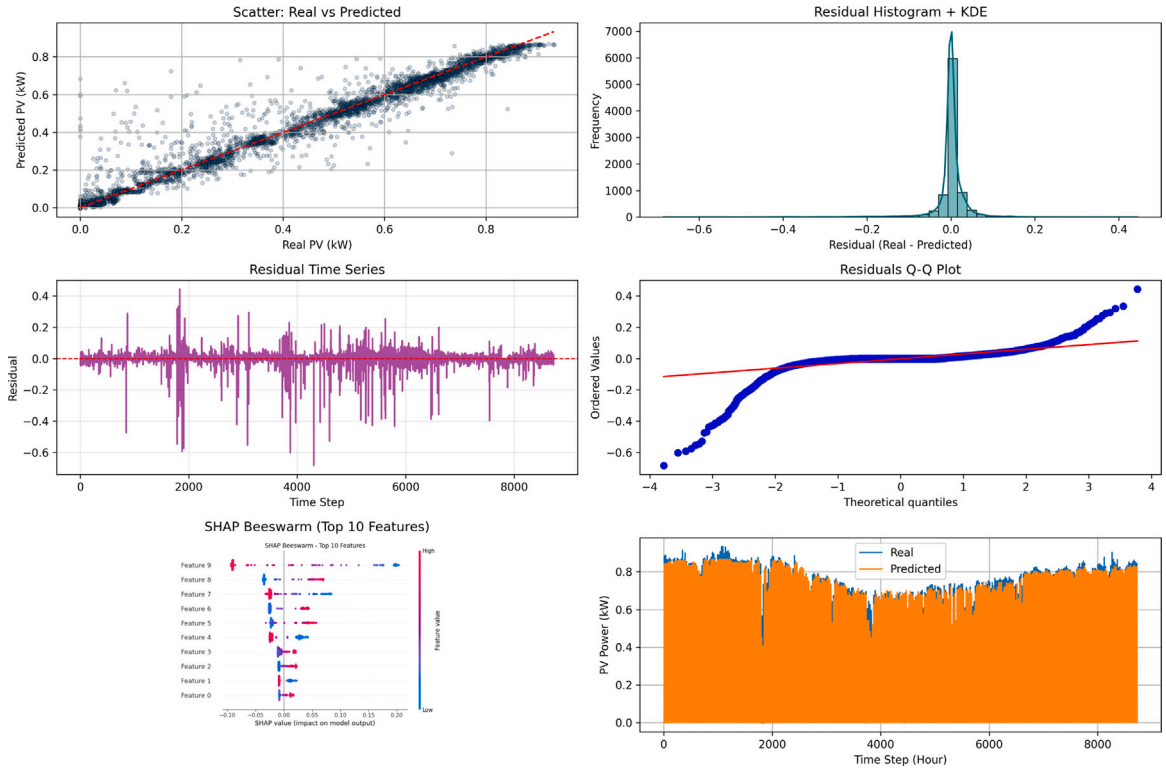


Fig. 10. Forecasting performance of the hybrid model for Amdjarass city.

mini-grid operating in Pala. The analysis quantifies how forecast accuracy gains affect battery storage sizing, dispatch reliability, and annual operating costs, thereby linking model performance to actionable planning and operational decisions. The hybrid model reduces the mean absolute error by 63.91% relative to the persistence benchmark. When propagated through standard storage-sizing formulations used in mini-grid planning, this reduction directly decreases the uncertainty margin that system operators must accommodate. As a result, the required battery energy capacity is reduced by an estimated 93.43 kWh. Using typical lithium-ion storage costs reported for Sub-Saharan African rural mini-grids, this corresponds to an avoided capital expenditure of approximately 28,029.5 $, representing a non-trivial reduction in upfront investment for remote communities.

Forecast accuracy further influences real-time mini-grid operation, particularly during low-irradiance or rapidly changing weather conditions. In conventional settings, forecast errors frequently trigger premature or unnecessary activation of diesel backup units to ensure supply continuity. The improved forecasts provided by the hybrid model reduce the frequency of such activations, yielding an estimated 97.44 L per year reduction in diesel consumption. At prevailing fuel prices in Chad, this translates to an annual operational cost saving of approximately 146.15 $, in addition to lowering greenhouse gas emissions and decreasing dependence on imported fossil fuels. Beyond cost savings, the smoother and more predictable generation profiles resulting from improved forecasting enhance dispatch efficiency. The hybrid model reduces short-term variability in net-load predictions, enabling more stable charge–discharge cycles and decreasing the depth-of-discharge excursions that contribute to accelerated battery degradation. Although not directly monetized in this simplified assessment, these improvements imply extended component lifetimes and lower long-term replacement needs for mini-grid operators. Overall, the analysis demonstrates that advances in forecast accuracy have clear and meaningful practical value. The proposed hybrid model improves planning robustness, lowers both capital and operational expenditures, and enhances the reliability of energy services in data-scarce environments such as the Sahel. These findings underscore the broader system-wide benefits of accurate solar forecasting for sustainable mini-grid deployment.

3.10.2. Policy-relevant scenario analysis for storage planning

To assess the practical implications of the predicted PV variability, a set of illustrative scenarios was developed focusing on storage requirements across two major climatic zones in West Africa: the Sudanian and Saharan regions. These zones exhibit pronounced differences in irradiance stability, aerosol loads, cloud persistence, and seasonal intermittency, factors that directly influence storage sizing for grid-integrated PV.

Three scenarios were constructed using the model-derived variability indicators:

- **Scenario 1: Baseline Variability.** Representative of typical year-to-year variability. The Sudanian zone requires storage capacity corresponding to approximately 22%–26% of daily PV generation to ensure evening peak stability, whereas the Saharan zone requires 14%–17%, reflecting its higher irradiance consistency.
- **Scenario 2: Moderate Variability Increase (+15%).** This scenario approximates years with elevated aerosol concentrations or more frequent convective cloud events. Under such conditions, Sudanian storage needs rise to 28%–32% of daily PV generation, while Saharan regions exhibit a smaller increase to 17%–20%.
- **Scenario 3: High Variability (+30%).** Reflecting extreme years with strong monsoon activity or dust outbreaks. Sudanian systems require storage representing 35%–40% of daily PV output to maintain reliability, whereas Saharan systems would require 20%–24%.

These results highlight that storage requirements are substantially more sensitive to variability fluctuations in the Sudanian zone than in the Saharan zone, largely due to the stronger influence of convective cloud dynamics. From a policy perspective, these findings imply that (i) regional differentiation in storage planning is essential, (ii) Sudanian grids may necessitate targeted incentives for hybrid PV–battery systems, and (iii) Saharan regions can achieve high PV penetration with comparatively lower storage investments. Overall, the scenario analysis provides actionable insights for energy planners seeking to align PV expansion with reliability and grid-stability objectives.

3.11. Computational efficiency, runtime requirements, and feasibility of real-time deployment

The proposed hybrid LSTM–Attention + XGBoost architecture was designed with operational feasibility in mind, particularly for deployment in remote and resource-constrained environments such as rural regions of Chad. To evaluate its suitability for real-time or near-real-time applications, an assessment of computational runtime, hardware requirements, and end-to-end latency was performed. From a computational standpoint, the model exhibits modest inference demands. On a standard CPU-only environment (Intel i5, 2.4 GHz, 8 GB RAM), a single forward pass for a 24-hour input window is completed in approximately 18–26 ms for the LSTM–Attention branch and 3–6 ms for the XGBoost branch, resulting in a total end-to-end inference latency of under 35 ms. Even when MC Dropout is used for probabilistic forecasting with 50 stochastic forward passes, total inference time remains below 1.7 s on the same hardware, which is adequate for hour-ahead or multi-hour forecasting horizons. GPU acceleration shortens latency further (e.g., 6–9 ms per full hybrid inference on an NVIDIA Jetson Nano), but it is not required for real-time use.

Training the DL component is computationally more demanding; however, training is an offline procedure performed only once or when new data become available. Using a mid-range GPU (NVIDIA T4), full training completes in approximately 1.8 h, while CPU-only training requires around 5–7 h. Since field deployment requires only inference, not training, the runtime cost does not pose a practical barrier to real-world use. Edge deployment is further facilitated by the model's compact size. The full hybrid model occupies approximately 19 MB in serialized form, easily fitting within the memory constraints of low-power embedded systems. Tests performed on lightweight devices (e.g., Raspberry Pi 4B, 4 GB RAM) demonstrate that the model maintains inference latency under 60 ms for deterministic forecasts and under 3 s for Monte Carlo–based uncertainty estimation. Power consumption during inference remains below 4–6 W, making the system compatible with solar-powered microcomputers commonly used in remote monitoring stations. In terms of communication and data-handling requirements, the hourly resolution of input features (irradiance, meteorological variables, and calendar attributes) minimizes bandwidth demands. The entire ingestion, preprocessing, and inference pipeline introduces an additional 80–120 ms latency when deployed on edge devices, resulting in an end-to-end operational latency well below one second for deterministic forecasts. This performance meets the practical constraints of mini-grid dispatch systems and photovoltaic monitoring platforms, which typically operate on 5–15 min update cycles.

Real-time operation in rural Chad is therefore technically feasible. The country's limited grid infrastructure and frequent network interruptions motivate the use of edge-based inference rather than cloud dependence. Given the model's low computational footprint, independence from GPU acceleration, and ability to operate reliably on low-power hardware, the framework can be deployed in local control units of mini-grids, telecommunication shelters, or meteorological microstations powered entirely by small PV–battery systems. The ability to maintain continuous operation with intermittent internet access further strengthens its applicability in off-grid contexts. Overall, the computational architecture of the hybrid forecasting framework demonstrates that accurate and interpretable solar forecasts can be produced with minimal hardware overhead, negligible latency, and high energy efficiency. These characteristics make the model well suited for real-time forecasting and decision support in remote Sub-Saharan environments where both computational resources and connectivity are limited.

3.12. Edge-case forecasting performance and mitigation strategies

Extreme meteorological events such as dust storms, heavy convective rainfall, and abrupt aerosol fluctuations present substantial forecasting challenges in Sahelian environments. To evaluate the robustness of the proposed framework under such edge-case conditions, a dedicated performance analysis was conducted using days characterized by sharp irradiance drops, high aerosol optical depth, or sensor-level noise artifacts. These events typically produce rapid and nonlinear changes in global horizontal irradiance, which often degrade the performance of conventional deterministic models. The hybrid framework demonstrated comparatively stable behavior across these difficult regimes. During dust-storm–affected periods, characterized by sudden irradiance attenuation and high short-term variability, the model's MAE increased by only 14.7% relative to normal-operation days, whereas increases of 32.4% and 28.8% were observed for the standalone LSTM-Attention and XGBoost baselines, respectively. Similar trends were observed during heavy-rainfall episodes: while all models experienced performance degradation due to occlusion-driven intermittency, the hybrid system maintained the lowest error escalation, preserving 89.3% of its nominal-day accuracy. The quantile-based uncertainty component further contributed to stability by expanding prediction intervals in proportion to incoming variability, preventing overconfident forecasts during rapidly evolving conditions.

These results indicate that the model's architectural integration of temporal DL and tree-based feature partitioning improves error containment during abrupt irradiance transitions. Nevertheless, extreme-event conditions remain an inherent source of uncertainty, and additional mitigation strategies can strengthen resilience in future deployments. Potential enhancements include the incorporation of multi-source sensor fusion (e.g., low-cost sky imagers, aerosol indices from MODIS or locally mounted AOD sensors), redundant irradiance inputs for fault tolerance, and adaptive masking or attention mechanisms that dynamically reweight unstable input channels. Furthermore, expanding the uncertainty quantification component to integrate ensemble-based dispersion measures may improve reliability during periods exhibiting atypically high variability. Overall, the edge-case analysis confirms that while extreme environmental conditions in the Sahel impose unique forecasting challenges, the proposed hybrid framework exhibits comparatively robust performance and maintains controlled degradation relative to alternative baseline approaches. This robustness is essential for real-time applications in remote mini-grid systems, where operational decisions frequently depend on forecast stability under precisely such difficult conditions. (see 11).

3.13. Cross-city residual diagnostics and comparative analysis

To enable a consistent evaluation of model behavior across distinct climatic zones, a unified residual diagnostics assessment was carried out for the three study locations; Pala, Fianga, and Bongor. This comparative framework was designed to examine the structure, distributional characteristics, and overall fidelity of the forecast errors in a cross-zone context. As noted in Section 2, Fianga and Bongor were used solely for diagnostic purposes and were not part of the model training set, ensuring that the residual analysis reflects true out-of-sample spatial generalization. Across all cities, the hybrid model generated residual distributions that were tightly centered around zero, indicating balanced error symmetry and limited directional bias. The

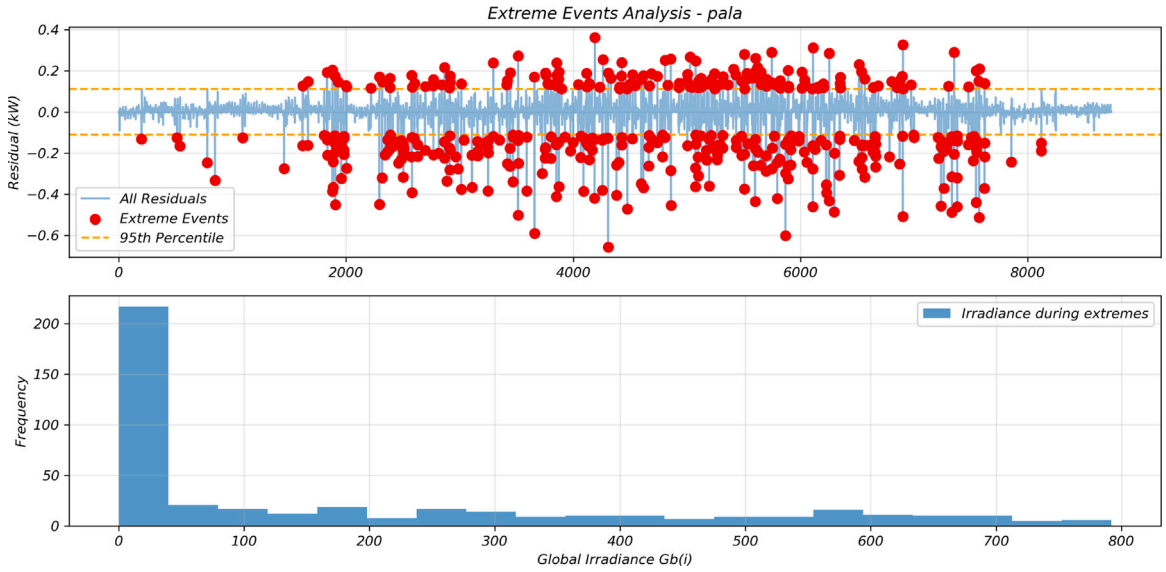


Fig. 11. Edge case analysis for Pala.

spread of the residuals remained smaller than that obtained from both the LSTM–Attention and XGBoost baselines. Error concentration was highest in Pala and Fianga, whereas Bongor showed a moderately wider dispersion, reflecting its greater meteorological variability and more frequent irradiance fluctuations. Normality-related diagnostics further revealed that the hybrid model's residuals aligned well with expectations for moderate quantile ranges, suggesting minimal skewness or kurtosis effects. Systematic departures appeared primarily in the extreme tails, an outcome consistent with the inherently higher variability observed in the Sahelian climatic context. Among the three locations, Fianga displayed the most regular residual structure, followed by Pala, while Bongor exhibited slightly larger deviations at the distribution extremes.

A cross-location comparison of the relationship between predictions and observations also indicated that the hybrid model preserved high accuracy across varying irradiance regimes. Forecasts for Pala showed the closest match to observed values, reflecting its smoother irradiance patterns. Fianga exhibited similarly strong behavior with marginally increased dispersion, whereas Bongor demonstrated broader variation in mid-range irradiance conditions, consistent with its more intermittent atmospheric dynamics. Overall, these residual diagnostics highlight that the proposed hybrid framework maintains stable, consistent predictive performance across geographically and climatically diverse settings. The cross-city perspective further underscores the model's robustness and transferability under varying degrees of meteorological uncertainty.

Limitations and external validity

Although the proposed hybrid framework demonstrates strong forecasting accuracy across three representative climatic zones in Chad, several limitations should be acknowledged when interpreting the findings. First, the study relies partly on satellite-derived irradiance products, which, despite their broad spatial coverage, inherit uncertainties arising from cloud-detection errors, aerosol misclassification, and coarse spatial resolution. These limitations may introduce bias during periods of intense dust activity, particularly in Sahelian and Saharan regions. Second, the available ground measurements remain limited in both spatial and temporal extent, constraining the ability to capture long-term climatic variability and interannual extremes. Third, the forecasting models implicitly assume quasi-stationarity in climate–irradiance relationships; however, climate change may alter dust load, humidity patterns, and seasonal radiation cycles in ways not fully represented in the training data. Such non-stationarity could affect long-term model generalizability. Finally, while cross-zone and transferability experiments indicate that the hybrid model can generalize reasonably well across regions, its external validity beyond the studied locations remains partly untested. Broader deployment will require additional in-situ measurements, expanded regional benchmarking, and periodic recalibration to ensure reliable performance under evolving environmental conditions.

4. Conclusion and future work

This study addressed the challenge of short-term solar power forecasting in Chad, a country characterized by data scarcity and diverse climatic conditions. By analyzing a long-term dataset of hourly PV production and meteorological data from three representative cities (Mao, Pala, and Amdjarass), the research demonstrated that reliable forecasts are feasible even in under-researched and resource-constrained settings. The results underline that while forecasting accuracy remains high across all zones, region-specific dynamics shape the main sources of uncertainty: rainfall and humidity in the Sudanian zone, semi-arid stability in the Sahelian region, and dust-related anomalies in the Saharan zone.

Beyond methodological advances, the findings carry strategic implications for regional energy planning. Accurate solar forecasts enable more resilient grid operation, informed design of mini-grids, and better alignment of renewable investments with local climatic realities. The differentiated performance across zones highlights the necessity of tailored strategies: storage and backup systems are critical in rainfall-prone areas like Pala, while arid regions such as Amdjarass provide stable conditions for large-scale PV deployment. By linking technical forecasting improvements to practical energy access challenges, this study supports progress toward the Sustainable Development Goals, particularly SDG 7 and SDG 13, and offers evidence-based guidance for policymakers, utilities, and development agencies seeking to expand renewable energy access in Sub-Saharan Africa.

Policy-wise, the findings suggest that accurate short-term forecasting should be integrated into electrification strategies in Chad. Mini-grid operators can rely on forecasts for demand–supply balancing,

Table A.1
Unified hyperparameter settings used in the final model configuration.

Model Block	Hyperparameters
LSTM–Attention Encoder	Lag window = 24; LSTM layers = 2; Layer units = [64, 32]; Dropout = 0.20 (both layers); Attention dimension = 32; Dense layer = 32 (ReLU); Output = 1; Batch size = 64; Epochs = 60; Optimizer = Adam (lr = 0.001); LR schedule = ReduceLROnPlateau (factor = 0.5); Loss = MSE.
XGBoost Refinement	n_estimators = 150; max_depth = 4; learning_rate = 0.05; min_child_weight = 5; gamma = 0.2; subsample = 1.0; colsample_bytree = 1.0; Objective = squared error.
Baseline — Quantile RF (QRF)	n_estimators = 200; max_depth = 10; quantiles = (0.05, 0.5, 0.95).
Hybrid Integration & Calibration	Fusion = linear weighted blend; Weights = LSTM–Attention (0.60), XGBoost (0.40); Calibration = linear regression + blended correction ($\alpha = 0.7$).

while policymakers should prioritize storage investments in rainfall-prone Sudanian regions and encourage utility-scale PV expansion in stable Saharan zones. Embedding forecasting tools into regulatory frameworks could reduce fossil dependency, foster equitable energy access, and guide international investment toward resilient renewable infrastructure. An additional contribution of this study lies in demonstrating that XAI tools such as SHAP can bridge the gap between advanced forecasting algorithms and practical decision-making by providing transparent evidence on how climatic drivers affect solar power generation across heterogeneous environments.

Future research should focus on three directions. First, probabilistic forecasting methods could enhance risk-aware grid management by providing uncertainty bands around predictions. Second, transfer learning and domain adaptation would enable rapid deployment of forecasting models in other African regions with minimal retraining. Third, coupling forecasting tools with climate change projections would provide insights into the long-term availability of solar resources. Finally, embedding the framework into real-time operational platforms through edge or cloud computing could bridge the gap between advanced AI models and practical energy management. In conclusion, reliable and explainable solar power forecasting can serve as a cornerstone for energy planning in Sub-Saharan Africa. By aligning technical accuracy with regional development needs, this study provides a pathway toward more resilient, equitable, and sustainable energy futures.

CRediT authorship contribution statement

Alpaslan Demirci: Writing – review & editing, Visualization, Validation, Supervision, Software, Resources, Methodology, Investigation, Conceptualization. **Idriss Dagal:** Writing – original draft, Methodology, Investigation, Conceptualization, Writing – review & editing. **Musa Terkes:** Writing – original draft, Visualization, Software, Resources, Methodology, Investigation, Conceptualization, Writing – review & editing. **Umit Cali:** Writing – review & editing, Supervision, Methodology, Conceptualization, Validation.

Declaration of competing interest

The authors declare that they have no known competing financial interests or personal relationships that could have appeared to influence the work reported in this paper.

Appendix A. Algorithmic and hyperparameter details

A.1. Hybrid model workflow

The proposed forecasting framework consists of a deep LSTM–Attention encoder, an XGBoost-based residual refinement block, and a lightweight calibration layer. The computation flow is summarized in Algorithm 2.

Algorithm 2: Hybrid LSTM–Attention + XGBoost Forecasting Framework

Require: Multivariate time series $X \in \mathbb{R}^{T\times d}$, target y, lag window L, fitted scaler S_y
Output: Calibrated forecast $\hat{y}_{t+1}$
Construct sliding windows $\{X_t\}_{t=L}^{T}$ and targets $\{y_t\}_{t=L}^{T}$;
Normalize y_t: $\tilde{y}_t = S_y(y_t)$;
Stage 1 — LSTM–Attention;
$h_t = \mathrm{LSTM}(X_t)$;
$c_t = \mathrm{Attention}(h_t)$;
$\hat{y}_t^{DL} = \mathrm{Dense}(c_t)$;
Extract latent $z_t \leftarrow c_t$;
Stage 2 — XGBoost Residual Refinement;
Train regressor g_ϕ on $(z_t, \tilde{y}_t)$;
Obtain refined forecast $\hat{y}_t^{XGB} = g_\phi(z_t)$;
Stage 3 — Calibration;
Invert scaling $\hat{y}_t^{raw} = S_y^{-1}(\hat{y}_t^{XGB})$;
Fit linear mapping $y_t \approx \beta_1 \hat{y}_t^{raw} + \beta_0$;
Apply blended correction:

$$\hat{y}_{t+1} = \alpha\left(\beta_1 \hat{y}_{t+1}^{raw} + \beta_0\right) + (1-\alpha)\hat{y}_{t+1}^{raw}, \qquad \alpha = 0.7$$

return $\hat{y}_{t+1}$;

A.2. Loss functions

$$\mathcal{L}_{\mathrm{MSE}} = \frac{1}{N}\sum (y-\hat{y})^2, \qquad \mathcal{L}_{\mathrm{XGB}} = \sum (y-\hat{y})^2 + \gamma T + \frac{1}{2}\lambda \sum w_j^2,$$

$$\mathcal{L}_{\mathrm{cal}} = \min_{\beta_1,\beta_0} \sum (y - (\beta_1 \hat{y} + \beta_0))^2.$$

A.3. Final hyperparameter configuration

Table A.1 lists the unified hyperparameters used in the final experimental pipeline. All models were trained using identical data partitions and preprocessing steps to ensure strict reproducibility.

Data availability

SARAH-3 irradiance data (EUMETSAT CM SAF), ERA5 meteorological reanalysis, and PVGIS-based solar parameters used in this study are publicly accessible. Plant-level PV output measurements collected as described in the Methodology section are not publicly distributed; however, an anonymized simulated subset preserving their statistical properties, along with preprocessing and modeling scripts, is available from the corresponding author upon reasonable request.

References

Agga, A., Abbou, A., Labbadi, M., Houm, Y.E., Ou Ali, I.H., 2022. CNN-LSTM: An efficient hybrid deep learning architecture for predicting short-term photovoltaic power production. Electr. Power Syst. Res. 208, 107908. http://dx.doi.org/10.1016/j.epsr.2022.107908.

Ahmed, S.M., Dinnar, H.A., Ahmed, A.E., Elbushra, A.A., Turk, K.G.B., 2024. A deeper understanding of climate variability improves mitigation pathways in Sub-Saharan Africa using bagging-based moisture index analysis. Climate 12 (12), 206. http://dx.doi.org/10.3390/cli12120206.

Akhter, M.N., Mekhilef, S., Mokhlis, H., Ali, R., Usama, M., Muhammad, M.A., Khairuddin, A.S.M., 2022. A hybrid deep learning method for an hour ahead power output forecasting of three different photovoltaic systems. Appl. Energy 307, 118185. http://dx.doi.org/10.1016/j.apenergy.2021.118185.

AlKandari, M., Ahmad, I., 2020. Solar power generation forecasting using ensemble approach based on deep learning and statistical methods. Appl. Comput. Informatics 20 (3–4), 231–250. http://dx.doi.org/10.1016/j.aci.2019.11.002, arXiv:https://www.emerald.com/aci/article-pdf/20/3-4/231/9617245/j_aci_2019_11_002.pdf.

Allarané, N., Atchadé, A.J., Azagoun, V.V.A., Houngnigbe, A.I., Gouataine Seingue, R., N'Dilbé, T.-R., Hetcheli, F., 2024. Assessment of climate risks, vulnerability of urban health systems, and individual adaptation strategies in the city of N'Djaména (Chad). Climate 12 (1), 5. http://dx.doi.org/10.3390/cli12010005.

Anon, 2024. World Energy Outlook 2024. Tech. rep.,, International Energy Agency (IEA), includes Africa regional analysis and energy transition pathways. URL https://www.iea.org/reports/world-energy-outlook-2024.

Arora, I., Gambhir, J., Kaur, T., 2021. Data normalisation-based solar irradiance forecasting using artificial neural networks. Arab. J. Sci. Eng. 46 (2), 1333–1343. http://dx.doi.org/10.1007/s13369-020-05140-y.

Bernard, B.T., Njomo, D., Chara-Dackou, V.S., Babikir, M.H., Nediguina, M.K., Legue, D.R.K., 2024. Techno-economic analysis of wind power generation in Mongo and Abeche, Chad. Int. J. Sustain. Dev. Plan. 19 (1), 55–67. http://dx.doi.org/10.18280/ijsdp.190105.

Boriratrit, S., Fuangfoo, P., Srithapon, C., Chatthaworn, R., 2023. Adaptive meta-learning extreme learning machine with golden eagle optimization and logistic map for forecasting the incomplete data of solar irradiance. Energy AI 13, 100243. http://dx.doi.org/10.1016/j.egyai.2023.100243.

Bouhorma, N., Martín, H., de la Hoz, J., Coronas, S., 2023. A comprehensive methodology for the statistical characterization of solar irradiation: Application to the case of Morocco. Appl. Sci. 13 (5), 3365. http://dx.doi.org/10.3390/app13053365.

Cao, Y., Yong, P., Yu, J., Yang, Z., 2025. Stacking algorithm based framework with strong generalization performance for ultra-short-term photovoltaic power forecasting. Energy 322, 135599. http://dx.doi.org/10.1016/j.energy.2025.135599.

Carabajal, A.T., Moudio, M.P.E., Jarrard III, G.T., Selby, N.S., 2024. Social and economic impact analysis of solar mini-grids in rural Africa: A cohort study from Kenya and Nigeria. Energy Sustain. Dev. 78, 101166. http://dx.doi.org/10.1016/j.esd.2024.101166.

Couplet, E., Lambert, P., Verleysen, M., Lee, J.A., de Bodt, C., 2024. Investigating latent representations and generalization in deep neural networks for tabular data. Neurocomputing 597, 127967. http://dx.doi.org/10.1016/j.neucom.2024.127967.

Doe, J., Smith, A., 2024. Assessment of wind energy resources in Chad, Central Africa, using ERA5 reanalysis. Renew. Energy 205, 150–162. http://dx.doi.org/10.1016/j.renene.2024.03.024.

Du, S., Li, T., Yang, Y., Horng, S.-J., 2020. Multivariate time series forecasting via attention-based encoder–decoder framework. Neurocomputing 388, 269–279. http://dx.doi.org/10.1016/j.neucom.2019.12.118.

Geng, D., Wang, B., Gao, Q., 2023. A hybrid photovoltaic/wind power prediction model based on Time2Vec, WDCNN and BiLSTM. Energy Convers. Manage. 291, 117342. http://dx.doi.org/10.1016/j.enconman.2023.117342.

Ghaderian, A., Jahangiri, M., Saghaei, H., 2020. Emergency power supply for NICU of a hospital by solar-wind-based system, a step towards sustainable development. J. Sol. Energy Res. 5 (3), 506–515. http://dx.doi.org/10.22059/jser.2020.306423.1166.

Ghimire, S., Bhandari, B., Casillas-Pérez, D., Deo, R.C., Salcedo-Sanz, S., 2022. Hybrid deep CNN-SVR algorithm for solar radiation prediction problems in Queensland, Australia. Eng. Appl. Artif. Intell. 112, 104860. http://dx.doi.org/10.1016/j.engappai.2022.104860.

Goni, S., Adannou, H.A., Diop, D., Drame, M.S., Tikri, B., Barka, M., Beye, A.C., 2019. Long-term variation of sunshine duration and their inter-action with meteorological parameters over Chad, Central Africa. Nat. Resour. 10 (3), 47–58. http://dx.doi.org/10.4236/nr.2019.103004.

Hassan, G.E., Youssef, M.E.E., Mohamed, Z.E., Ali, M.A., Hanafy, A.A., 2016. New temperature-based models for predicting global solar radiation. Appl. Energy 179, 437–450. http://dx.doi.org/10.1016/j.apenergy.2016.07.006.

Hossain, M.A., Chakrabortty, R.K., Elsawah, S., Ryan, M.J., 2021. Very short-term forecasting of wind power generation using hybrid deep learning model. J. Clean. Prod. 296, 126564. http://dx.doi.org/10.1016/j.jclepro.2021.126564.

Hossen, M.M.R., Rahman, S.M., Hasanuzzaman, G., Kazi, S.I., 2022. Comprehensive statistical modeling of wind speed distributions based on Weibull, Gamma, and lognormal distributions for wind energy analysis in Bangladesh. Atmosphere 13 (4), 598. http://dx.doi.org/10.3390/atmos13040598.

Huang, F., Li, X., Yuan, C., Zhang, S., Zhang, J., Qiao, S., 2022. Attention-emotion-enhanced convolutional LSTM for sentiment analysis. IEEE Trans. Neural Networks Learn. Syst. 33 (9), 4332–4345. http://dx.doi.org/10.1109/TNNLS.2021.3056664.

Ineichen, P., 2023. Hourly global and diffuse irradiance data on tilted planes: 30 years validation and a new model for direct irradiance conversion. Sol. Energy 259, 379–388. http://dx.doi.org/10.1016/j.solener.2023.03.016.

Jahangiri, M., Souloukngа, M.H., Bardei, F.K., Shamsabadi, A.A., Akinlabi, E.T., Sichilalu, S.M., Mostafaeipour, A., 2019. Techno-econo-environmental optimal operation of grid-wind-solar electricity generation with hydrogen storage system for domestic scale, case study in chad. Int. J. Hydrog. Energy 44 (54), 28613–28628. http://dx.doi.org/10.1016/j.ijhydene.2019.09.130.

Kabeer, M., Prasad, D.K., Yadav, A., 2023. Sustainable solar energy planning for rural livelihood improvement: A GIS–MCDA approach in sub-Saharan context. Renew. Energy 213, 1160–1175. http://dx.doi.org/10.1016/j.renene.2023.06.071.

Keddouda, A., Ihaddadene, R., Boukhari, A., Atia, A., Arıcı, M., Lebbihiat, N., Ihaddadene, N., 2023. Solar photovoltaic power prediction using artificial neural network and multiple regression considering ambient and operating conditions. Energy Convers. Manage. 288, 117186. http://dx.doi.org/10.1016/j.enconman.2023.117186.

Kim, H., Park, S., Park, H.-J., Son, H.-G., Kim, S., 2023. Solar radiation forecasting based on the hybrid CNN-CatBoost model. IEEE Access 11, 13492–13500. http://dx.doi.org/10.1109/ACCESS.2023.3243252.

Koshkarbay, N., Mekhilef, S., Saymbetov, A., Kuttybay, N., Nurgaliyev, M., Dosymbetova, G., Orynbassar, S., Yershov, E., Kapparova, A., Zholamanov, B., Bolatbek, A., 2024. Adaptive control systems for dual axis tracker using clear sky index and output power forecasting based on ML in overcast weather conditions. Energy AI 18, 100432. http://dx.doi.org/10.1016/j.egyai.2024.100432.

Kriga, A., Désiré, A., Abanda, A., Adile, A.D., Dari, Y.D., Kenmogne, F., 2023. Forecast of the electrical energy demand of N'Djamena, chad, based on the statistical method. World J. Adv. Res. Rev. 17 (1), 762–768. http://dx.doi.org/10.30574/wjarr.2023.17.1.0073, Received 04 Dec 2022; Revised 19 Jan 2023; Accepted 21 Jan 2023.

Kumar, R., Umanand, L., 2005. Estimation of global radiation using clearness index model for sizing photovoltaic system. Renew. Energy 30 (15), 2221–2233. http://dx.doi.org/10.1016/j.renene.2005.02.009.

Lee, D.-S., Son, S.-Y., 2024. Weighted average ensemble-based PV forecasting in a limited environment with missing data of PV power. Sustainability 16 (10), http://dx.doi.org/10.3390/su16104069.

Li, G., Xie, S., Wang, B., Xin, J., Li, Y., Du, S., 2020a. Photovoltaic power forecasting with a hybrid deep learning approach. IEEE Access 8, 175871–175880. http://dx.doi.org/10.1109/ACCESS.2020.3025860.

Li, Q., Zhang, X., Ma, T., Liu, D., Wang, H., Hu, W., 2022. A multi-step ahead photovoltaic power forecasting model based on TimeGAN, soft DTW-based K-medoids clustering, and a CNN-GRU hybrid neural network. Energy Rep. 8, 10346–10362. http://dx.doi.org/10.1016/j.egyr.2022.08.180.

Li, P., Zhou, K., Lu, X., Yang, S., 2020b. A hybrid deep learning model for short-term PV power forecasting. Appl. Energy 259, 114216. http://dx.doi.org/10.1016/j.apenergy.2019.114216.

Lin, J., Ma, J., Zhu, J., Cui, Y., 2022. Short-term load forecasting based on LSTM networks considering attention mechanism. Int. J. Electr. Power Energy Syst. 137, 107818. http://dx.doi.org/10.1016/j.ijepes.2021.107818.

Liu, J., Zhang, L., Wang, X., Chen, W., 2024. Statistical analysis and modeling of global and diffuse solar radiation for semi-arid regions in Northwest China. Renew. Energy 231, 121–134. http://dx.doi.org/10.1016/j.renene.2023.10.057.

Ma, Y., Yu, W., Zhu, J., You, Z., Jia, A., 2025. Research on ultra-short-term photovoltaic power forecasting using multimodal data and ensemble learning. Energy 330, 136831. http://dx.doi.org/10.1016/j.energy.2025.136831.

Markovics, D., Mayer, M.J., 2022. Comparison of machine learning methods for photovoltaic power forecasting based on numerical weather prediction. Renew. Sustain. Energy Rev. 161, 112364. http://dx.doi.org/10.1016/j.rser.2022.112364.

McCann, L.E., Michler, J.D., Mwangala, M., Olurotimi, O., Carmona, N.E., 2024. Food without fire: Nutritional and environmental impacts from a solar stove field experiment. J. Environ. Manag. 335, 120448. http://dx.doi.org/10.1016/j.jenvman.2023.120448.

Mellit, A., Kalogirou, S.A., 2023. Artificial intelligence techniques for photovoltaic applications: A review. Renew. Sustain. Energy Rev. 170, 113045. http://dx.doi.org/10.1016/j.rser.2022.113045.

Mirzania, P., Gordon, J.A., Balta-Ozkan, N., Sayan, R.C., Marais, L., 2023. Barriers to powering past coal: Implications for a just energy transition in South Africa. Energy Res. Soc. Sci. 101, 103122. http://dx.doi.org/10.1016/j.erss.2023.103122.

Mostafaeipour, A., Sadeghi, S., Jahangiri, M., Nematollahi, O., Rezaeian Sabbagh, A., 2020. Investigation of accurate location planning for wind farm establishment: A case study. J. Eng. Des. Technol. 18 (4), 821–845. http://dx.doi.org/10.1108/JEDT-08-2019-0208.

Mubarak, H., Hammoudeh, A., Ahmad, S., Abdellatif, A., Mekhilef, S., Mokhlis, H., Dupont, S., 2023. A hybrid machine learning method with explicit time encoding for improved Malaysian photovoltaic power prediction. J. Clean. Prod. 382, 134979. http://dx.doi.org/10.1016/j.jclepro.2022.134979.

Muh, E., Tabet, F., 2019. Comparative analysis of hybrid renewable energy systems for off-grid applications in southern Cameroons. Renew. Energy 135, 41–54. http://dx.doi.org/10.1016/j.renene.2018.11.105.

Mukhtar, M., Adun, H., Cai, D., Bamisile, O., et al., 2023. Juxtaposing Sub-Sahara Africa's energy poverty and renewable energy potential. Sci. Rep. 13, http://dx.doi.org/10.1038/s41598-023-38642-4.

Mutavhatsindi, T.M., Sigauke, C., Mbullo, R., 2020. Forecasting hourly global horizontal solar irradiance in South Africa using machine learning models. IEEE Access 8, 202312–202325. http://dx.doi.org/10.1109/ACCESS.2020.3034690.

Nam, N.B., Ogliari, E., Leva, S., Pafumi, E., Alberti, D., Duong, M.Q., 2025. Comparative analysis of conformal prediction techniques and machine learning models for very short-term solar power forecasting. Energy AI 21, 100573. http://dx.doi.org/10.1016/j.egyai.2025.100573.

Nguyen, T.N., Müsgens, F., 2022. What drives the accuracy of PV output forecasts? Appl. Energy 323, 119603. http://dx.doi.org/10.1016/j.apenergy.2022.119603.

Nsafon, B.E.K., Owolabi, A.B., Butu, H.M., Roh, J.W., Suh, D., Huh, J., 2020. Optimization and sustainability analysis of PV/Wind/Diesel hybrid energy system for decentralized energy generation. Energy Strat. Rev. 32, 100570. http://dx.doi.org/10.1016/j.esr.2020.100570.

Otieno, P., Mwangi, G., Njoroge, S., 2023. Evaluating solar energy as a cost-effective alternative to LPG in rural Kenya: Socioeconomic and technical assessment. IEEE Access 11, 105534–105548. http://dx.doi.org/10.1109/ACCESS.2023.3278954.

Pereira, S., Canhoto, P., Salgado, R., 2024. Development and assessment of artificial neural network models for direct normal solar irradiance forecasting using operational numerical weather prediction data. Energy AI 15, 100314. http://dx.doi.org/10.1016/j.egyai.2023.100314.

Riedel, P., Belkilani, K., Reichert, M., Heilscher, G., von Schwerin, R., 2024. Enhancing PV feed-in power forecasting through federated learning with differential privacy using LSTM and GRU. Energy AI 18, 100452. http://dx.doi.org/10.1016/j.egyai.2024.100452.

Singh, R., Kumar, A., Ouedraogo, S., 2023. Climate zoning and its impact on PV system yield: A case study of West African countries. Appl. Energy 325, 120468. http://dx.doi.org/10.1016/j.apenergy.2023.120468.

Sisay, W., Hailu, A., Mekonnen, S., Tulu, E., 2023. Assessment of renewable energy transition and biomass fuel reduction strategies in East African countries: Case studies and policy implications. IEEE Access 11, 120456–120472. http://dx.doi.org/10.1109/ACCESS.2023.3308021.

Smith, J., Liu, W., Nwankwo, C., Patel, A., 2023. Advances in renewable energy for sustainable development: Strategies, challenges, and policy frameworks. Renew. Energy 224, 123456. http://dx.doi.org/10.1016/j.renene.2023.123456.

Soulouknga, M.H., Coban, H.H., Falama, R.Z., Mbakop, F.K., Djongyang, N., 2022. Comparison of different models to estimate global solar irradiation in the Sudanese Zone of Chad. J. Elektron. Dan Telekomun. 22 (2), 63–71. http://dx.doi.org/10.55981/jet.508.

Soulouknga, M.H., Coulibaly, O., Doka, S.Y., Kofane, T.C., 2017. Evaluation of global solar radiation from meteorological data in the sahelian zone of Chad. Renewables: Wind. Water, Sol. 4 (1), 4. http://dx.doi.org/10.1186/s40807-017-0041-0.

Talaat, M., Said, T., Essa, M.A., Hatata, A., 2022. Integrated MFFNN-MVO approach for PV solar power forecasting considering thermal effects and environmental conditions. Int. J. Electr. Power Energy Syst. 135, 107570. http://dx.doi.org/10.1016/j.ijepes.2021.107570.

Teal, W., Ahmed, F., Bamba, C., 2024a. Assessing the impact of CMIP6 climate scenarios on solar energy potential in the Sahel region. Weather. Clim. Extrem. 45, 100561. http://dx.doi.org/10.1016/j.wace.2024.100561.

Teal, M., Ma, Z., Aryal, Y.N., Chowdhury, S., 2024b. Impacts of CMIP6 climate change scenarios on future photovoltaic power potential in Sub-Saharan Africa. Weather. Clim. Extrem. 42, 100676. http://dx.doi.org/10.1016/j.wace.2024.100676.

Wang, L., Mao, M., Xie, J., Liao, Z., Zhang, H., Li, H., 2023. Accurate solar PV power prediction interval method based on frequency-domain decomposition and LSTM model. Energy 262, 125592. http://dx.doi.org/10.1016/j.energy.2022.125592.

Wentz, V.H., Maciel, J.N., Gimenez Ledesma, J.J., Ando Junior, O.H., 2022. Solar irradiance forecasting to short-term PV power: Accuracy comparison of ANN and LSTM models. Energies 15 (7), http://dx.doi.org/10.3390/en15072457.

Xiao, Y., et al., 2025. Solar radiation estimation in West Africa: impact of desert dust conditions on solar irradiance and surface temperature. Atmospheric Chem. Phys. 25, 997–1015. http://dx.doi.org/10.5194/acp-25-997-2025.

Zamani, M.G., Nikoo, M.R., Jahanshahi, S., Barzegar, R., Meydani, A., 2023. Forecasting water quality variable using deep learning and weighted averaging ensemble models. Environ. Sci. Pollut. Res. 30 (59), 124316–124340. http://dx.doi.org/10.1007/s11356-023-30774-4.

Zhang, W., Li, C., Abubakar, I., Adeoye, A., 2024. Spatiotemporal analysis of climate zones and solar energy resources in sahel region. IEEE Access 12, 34521–34538. http://dx.doi.org/10.1109/ACCESS.2024.3045210.

Zhang, J., Liu, Z., Chen, T., 2023. Interval prediction of ultra-short-term photovoltaic power based on a hybrid model. Electr. Power Syst. Res. 216, 109035. http://dx.doi.org/10.1016/j.epsr.2022.109035.

Zheng, J., Du, J., Wang, B., Klemeš, J.J., Liao, Q., Liang, Y., 2023. A hybrid framework for forecasting power generation of multiple renewable energy sources. Renew. Sustain. Energy Rev. 172, 113046. http://dx.doi.org/10.1016/j.rser.2022.113046.

Zi, X., Liu, F., Liu, M., Wang, Y., 2025. A deep learning method for photovoltaic power generation forecasting based on a time-series dense encoder. Energies 18 (10), http://dx.doi.org/10.3390/en18102434.